Wiley
Indoor Air
Volume 2025, Article ID 7436897, 29 pages
https://doi.org/10.1155/ina/7436897

WILEY

Research Article

Numerical Simulation on the Transmission Risk of SARS-CoV-2 During a Typical Elevator Ride

Hongyu Wu[1], **Hui An**[2] **and Simon Ching Man Yu**[1]

[1]*Department of Aeronautical and Aviation Engineering, The Hong Kong Polytechnic University, Hong Kong, Hong Kong, China*
[2]*Engineering Cluster, Singapore Institute of Technology, Singapore, Singapore*

Correspondence should be addressed to Hongyu Wu; hong-yu.wu@connect.polyu.hk

Received 27 September 2024; Accepted 20 May 2025

Academic Editor: Poulami Jha

Throughout the COVID-19 pandemic, several cases of infection associated with elevator rides have been reported. To systematically assess the risk of droplet transmission in an elevator, this study employed computational fluid dynamics (CFD) together with a modified stochastic dose–response model to quantify the infection risk for occupants. Simulation is conducted during a 2-min elevator ride for two individuals facing each other, without considering mask-wearing. Various factors such as ventilation outlet position, ventilation rates, air temperature, relative humidity, ventilation techniques, breathing patterns, and body types have been analyzed in order to assess the inhalation risks for occupants. Their infection probabilities for different viral strains are also considered. The findings highlight the effectiveness of the top-to-bottom ventilation approach. Nasal breathing has risk-reducing benefits, and ventilation rates of 30–50 air changes per hour (ACH) play an important role in reducing the risk of infection. Moreover, the study further reveals that air curtain systems outperform side ventilation. Temperature, relative humidity, the infected individual's breathing behavior, and the body types between infected and exposed individuals are shown to exert various degrees of influence on droplet transmission.

Keywords: aerosols; computational fluid dynamics; indoor space; infection probability; stochastic dose–response model; virus propagation

1. Introduction

For the past millennia, humanity has endured numerous extreme pandemics that have claimed millions of lives, leaving profound impacts on human populations and psychological aspects such as anxiety, social behavior, prolonged grief disorder, and coping mechanisms [1, 2]. It has been almost 4 years since the World Health Organization (WHO) first declared COVID-19 a pandemic. As of March 2025, the WHO reports that COVID-19 has resulted in 7.09 million deaths [3]. Although the peak of the pandemic has passed, sporadic infections and confirmed cases continue to occur. Research indicates that COVID-19 primarily spreads through contact with contaminated surfaces, droplets ($>100\,\mu$m) expelled by infected individuals through breathing, coughing, or sneezing, and smaller droplets or aerosols ($<100\,\mu$m) in the air [4, 5]. The prevailing scientific consensus is that the SARS-CoV-2 virus primarily targets the upper respiratory tract as well as the mucosa of the nasal, conjunctiva, or oral regions, where it can replicate rapidly [6]. Therefore, most transmission appears to occur through exposure to respiratory droplets or aerosols from an infected person in close contact.

During intense respiratory actions (coughing, sneezing, etc.), the human body generates a multitude of droplets that carry a plethora of viruses. These droplets can be transmitted through air over significant distances and can stay aloft for a long time. Studies indicate that a single cough can produce between 2085 and 5000 droplets, with sizes ranging from 1 to 1500 μm [7, 8]. A sneeze can even release between 40,000 and 1,000,000 droplets, measuring from 1 to 1000 μm in diameter [8, 9], potentially at speeds of up to 20 m/s [10]. The viral load of SARS-CoV-2 in these droplets can reach up to 2.35×10^9 copies/mL [11]. Smaller droplets

(< 75 μm) have a very fast momentum response time, allowing them to quickly follow the exhaled airflow, but their settling velocity is slower, enabling them to remain suspended in the air for a long time. Very large droplets (> 400 μm) maintain their speed due to their slower momentum response time. Despite their high settling velocity, their horizontal average velocity is large, allowing them to travel greater distances. Both types of droplets, under the influence of coughing airflow, travel over 2 m. Medium-sized droplets (75–400 μm) travel the shortest distance. Their settling velocity is more than 10 times that of smaller droplets, but their horizontal average velocity is much lower than that of larger droplets, leading to a shorter travel distance [4].

According to some previous studies, the risk of SARS-CoV-2 transmission is higher in enclosed spaces with poor ventilation, such as corridors [12] and restaurants [13]. There have also been many reports of infection incidents in elevators [14]. People living in urban environments frequently use elevators, and these confined spaces with high occupancy density provide favorable conditions for the spread of SARS-CoV-2.

In these environments, ventilation systems play a crucial role in removing contaminants and reducing exposure risk [15]. Although current standards require elevators to have designated ventilation areas and ventilation devices [16–18], there is a lack of specific guidelines for the rational design of ventilation volume and methods. Furthermore, research assessing the risk of virus transmission in these settings is still limited.

Current research on droplet transmission in elevators has certain limitations, with some influencing factors not fully considered. Van et al. [19] experimentally demonstrated early in the pandemic that increasing the elevator door open time can reduce the purification time of aerosols inside the elevator. However, they did not simulate the human exposure risk. Shao et al. [20] assessed the risk of airborne virus transmission in enclosed spaces such as elevators but only considered the impact of two low-risk respiratory behaviors—breathing and talking—under one ventilation mode. Sen et al. [21] simulated droplet dispersion in various scenarios within an elevator, including the number of coughing individuals, cough direction, and environmental relative humidity and temperature. Nonetheless, Sen et al. only evaluated risk based on the distribution of droplets at different locations, without considering the inhalation risk for susceptible individuals. Biswas et al. [22] and Dbouk et al. [23] modeled droplet dispersion under different ventilation scenarios (vent location and mode), but their models were limited to one infected individual and did not account for the exposure risk to susceptible populations. Li et al. [24] investigated the spread of cough-generated droplet aerosols and the exposure risk to inhalers under three ventilation modes but did not consider the impact of different human body shapes. Other respiratory behaviors or environmental temperature and relative humidity were not considered. Liu et al. [25] examined the effects of different standing positions and postures, as well as ventilation rates in elevators on infection risk. They only compared two ventilation rates and did not take account of different human body shapes, other respiratory behaviors, or environmental temperature and relative humidity. Based on current research and existing products, elevator ventilation systems can be categorized by vent location into two types: side ventilation [23, 24] and top ventilation [20–22]. Li et al. evaluated the effects of three ventilation modes (mixed ventilation (MV), displacement ventilation (DV), and air curtain ventilation (ACV)) on droplet purification and found that DV had poorer purification performance, while ACV was more effective [24]. However, to date, no research has systematically evaluated these ventilation methods to provide the optimal choice.

As mentioned above, no systematic research has yet been conducted to evaluate the impact of temperature, relative humidity, ventilation methods, respiratory behaviors, and individuals' height and body shape on the transmission risk of the SARS-CoV-2 virus. There is an urgent need to quantify the optimal ventilation rate and identify suitable ventilation strategies. Moreover, these studies have not considered the attenuation of the virus during transmission or the exposure probability of susceptible populations. The aim of this paper is to use computational fluid dynamics (CFD) together with a modified stochastic dose–response model to assess the exposure probability of individuals under various conditions and to determine appropriate ventilation settings.

The aim of this study is to evaluate the risk of droplet transmission in elevators and to determine appropriate ventilation strategies. The structure of this article is as follows: Section 2 provides a detailed overview of the computational methods used in this study, including model and case design, program information, boundary conditions, and infection probability models. Section 3 conducts a detailed analysis of the results from various cases and discusses the limitations of the current research as well as suggestions for future studies. Finally, brief concluding remarks are presented in Section 4.

2. Methodology

This section primarily outlines the methodology employed in this study, encompassing the model structural parameters, boundary conditions, case design, and the simulation models. It will also include the mathematical model used to evaluate the risk of exposure to infection within an elevator environment.

2.1. Model and Case Design. This study employs an elevator with dimensions of 2.5 m in height, 2 m in length, and 1.65 m in width. This is similar to elevators found in commercial and residential buildings. It typically has a maximum load capacity ranging from 1200 to 1600 kg and can accommodate 12–16 people [25]. Due to the height restrictions of residential and commercial buildings, the elevator ride duration was set to 2 min. To account for more hazardous viral transmission scenarios within the elevator, this study considers only two individuals standing face to face at fixed positions.

Table 1 shows all cases considered. Case 1 serves as the base case, as shown in Figure 1a. The ventilation structure features air outlets at the bottom and inlets at the top, with the pink and green human models representing the source and exposed individuals, both standing at a height of 1.75 m. The width of the air outlet and inlet is 0.02 and 0.05 m, respectively. The ventilation rate is set at 20 air changes per hour (ACH). This is the minimum ventilation standard required by the Elevator Design Code of the Hong Kong Special Administrative Region [17]. This higher ventilation rate is necessary because elevators are small, densely occupied spaces, which often require more frequent air changes [25, 26] compared to indoor offices or lecture halls. The temperature and relative humidity are set at 27°C and 50%, respectively, falling within the comfortable range for humans.

Group I (Cases 1–4) investigates the influence of ventilation outlet positions (OPs) on virus transmission, as illustrated by the schematic diagram in Figure 1b. The width of the vents remains constant. Blue indicates air inlets while red indicates air outlets. Four different positions for air outlets are tested: bottom, bottom middle, middle, and top. For the first three scenarios, the air conditioning inlet is located on the side of the elevator's top. In the scenario where the outlet is at the top, the inlet is positioned at the bottom side of the elevator to simulate DV.

Cases 5–9 in Group II consider the impact of different ventilation rates, ranging from 3 ACH (low infiltration scenario, air conditioning off) to 72 ACH (maximum air conditioning ventilation rate, equivalent to the minimum airflow required for 16 people in a floor area of 3.3 m^2 [27]), corresponding to mechanical ventilation rates from 0.0065 to 0.161 m^3/s and inlet velocities of 0.019–0.452 m/s.

Group III (Cases 10–15) studies the impact of different temperatures and relative humidity on the amount of virus inhaled by the exposed individual in the elevator. Based on elevator design standards in Hong Kong SAR [17], this study sets a temperature range of 5°C–37°C and a relative humidity range of 30%~95%.

Group IV (Cases 16–17) examines the differences in virus transmission between ACV and side ventilation, as shown in Figure 1c. The centralized ACV has an inlet diameter of 350 mm, set as a constant speed inlet. The distributed ACV uses a linear nozzle with dimensions of 30×460 mm, with ventilation volume and outlet dimensions and locations consistent with the baseline case.

Group V (Cases 18–20) involves the infected individual performing different respiratory patterns (RPs), including coughing, speaking loudly, sneezing, and sequential coughing (sequential coughing is defined as one cough followed quickly by the next), which produce virus clouds with different initial velocities and particle size distributions.

Finally, Group VI (Cases 21–23) examines virus transmission across various body types, utilizing adult man and child as source as well as adult man, adult woman, and child as exposed individual. The height of an adult man is set to 1.75 m, the height of an adult woman is set to 1.55 m, and the height of a child is set to 1.3 m. Additionally, all groups will consider the situation in which the exposed individual breathes through their noses and mouths separately.

2.2. Boundary Conditions. Table 2 summarizes the boundary conditions for the baseline scenario. The inlet adopts a uniform velocity, set to exchange air 20 times per hour. Air at a velocity of 0.126 m/s, temperature of 27°C, and relative humidity of 50% is supplied by a side-mounted air conditioner, entering vertically at the inlet face. The initial relative humidity and temperature of the indoor airflow are set to match the relative humidity and temperature of the ventilation system's air supply. According to previous studies [24], the initial turbulence kinetic energy was set to 9.5×10^{-5} m^2/s^2, and the initial turbulence dissipation rate was at 0.00185 m^2/s^3. Mouth1 represents the mouth of the infected person, where user defined function (UDF) 1 can represent velocity of coughing, sneezing, speaking loudly, and sequential coughing [10, 30, 31], as shown in Figure 2a. Mouth2 refers to the mouth of the exposed individual, with UDF2 representing the respiratory rate, following a sinusoidal function. The direction of respiratory activity through the mouth coincides with the horizontal direction (Y direction). Nose1 and Nose2 represent the noses of the infected and exposed individuals, respectively. During nasal breathing, the angle between the airflow direction and the horizontal direction is 60°. Their breathing frequency and velocity follow UDF3, which is another sine curve. Due to the differences in respiratory areas between the nose and mouth, the peak velocity is different, ensuring the same breathing volume, as shown in Figure 2b. Respiratory volume and frequency are related to body height and weight; thus, the respiratory boundary conditions for different body models in this study are calculated based on Gupta's theory [30]. With changes in body type, the duration of coughing remains unchanged, but the peak flow rate of the cough varies proportionally with body surface area (BSA). Similarly, the minute volume of breathing has a linear relationship with BSA. For males, the respiratory frequency is related to height and weight, with a decrease in height and an increase in weight leading to a higher respiratory rate; in this study, the weight for adult males is set at 65 kg, which falls within the healthy range of the body mass index (BMI). For females and children, the respiratory frequency is only related to height; as height decreases, respiratory rate increases. Consequently, a child's respiratory rate is higher than that of an adult woman, and an adult woman has a higher rate than adult men. And the minimum respiratory volume is seen in children, while adult males have the highest. It is important to note that in this study, the respiratory area for adult females and children is scaled down according to the square of their height proportion. Additionally, as infected individuals generally exhale at slightly higher temperatures during periods of heightened immune system activity, the exhaled gas temperature is slightly higher than that of uninfected individuals. All inlet velocities for the discrete phase are set to reflect, while discrete phase boundary conditions for all wall types are set to trap and fixed as a no-slip interface. The outlet is set to outflow, with discrete phase boundary conditions set to escape. Once particles deposit on the wall or escape from the computational domain through the outlet, the computational program will stop tracking the trajectory of these particles.

TABLE 1: Summary of all cases considered.

Case		Ventilation inlet position	Ventilation outlet position	Ventilation rate (ACH)	Temperature (°C) of supplied air	Relative humidity (%) of supplied air	Respiratory pattern (source)	Body type (source: Exposed)
I. Ventilation outlet position	1	Top	Bottom	20	27	50	Coughing	Adult man: Adult man
	2	Top	Middle	20	27	50	Coughing	Adult man: Adult man
	3	Top	Bottom middle	20	27	50	Coughing	Adult man: Adult man
	4	Bottom	Top	20	27	50	Coughing	Adult man: Adult man
II. Ventilation rate (ACH)	5	Top	Bottom	3	27	50	Coughing	Adult man: Adult man
	6	Top	Bottom	10	27	50	Coughing	Adult man: Adult man
	7	Top	Bottom	30	27	50	Coughing	Adult man: Adult man
	8	Top	Bottom	50	27	50	Coughing	Adult man: Adult man
	9	Top	Bottom	72	27	50	Coughing	Adult man: Adult man
III. Temperature and relative humidity	10	Top	Bottom	20	5	50	Coughing	Adult man: Adult man
	11	Top	Bottom	20	15	50	Coughing	Adult man: Adult man
	12	Top	Bottom	20	31	50	Coughing	Adult man: Adult man
	13	Top	Bottom	20	37	50	Coughing	Adult man: Adult man
	14	Top	Bottom	20	27	30	Coughing	Adult man: Adult man
	15	Top	Bottom	20	27	95	Coughing	Adult man: Adult man
IV. Ventilation methods	16	Central fan (top)	Bottom	20	27	50	Coughing	Adult man: Adult man
	17	Distributed fan (top)	Bottom	20	27	50	Coughing	Adult man: Adult man
V. Respiratory patterns of infected individual	18	Top	Bottom	20	27	50	Sneezing	Adult man: Adult man
	19	Top	Bottom	20	27	50	Speaking loudly	Adult man: Adult man
	20	Top	Bottom	20	27	50	Sequential coughing	Adult man: Adult man
VI. Body type	21	Top	Bottom	20	27	50	Coughing	Adult man: Adult woman
	22	Top	Bottom	20	27	50	Coughing	Adult man: Child
	23	Top	Bottom	20	27	50	Coughing	Child: Child

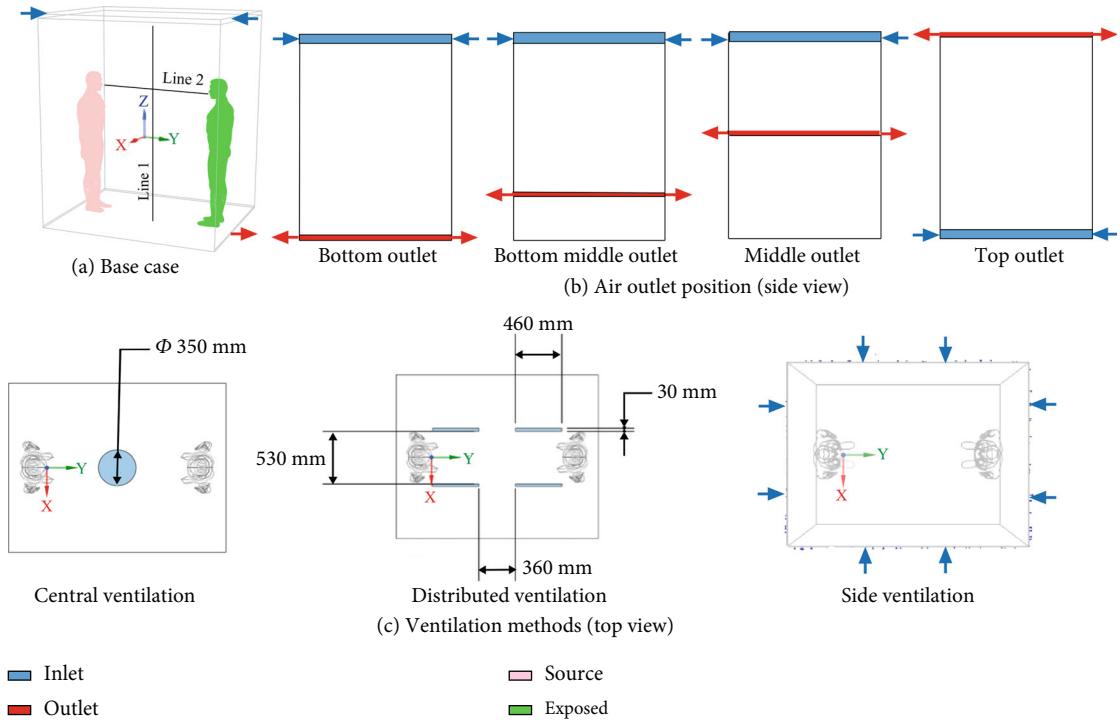

Figure 1: Case considered (refer to Table 1).

This study assumes that within 120 s of riding together in an elevator, there is only one exposure between the infectious source and the exposed individual, starting from the time when the virus begins to spread from the source. Subsequently, the two body models begin asynchronous breathing, with the infectious source utilizing nasal breathing. The exposed individual starts nasal or oral breathing from 0 s onward. The nasal and oral breathing areas are 0.6 and 1.2 cm^2, respectively. Oral breathing is in the horizontal plane, while nasal breathing has a mean side angle of 60°. In the fifth scenario, particle sources include coughing, sneezing, speaking loudly, and secondary coughing. The boundary conditions for each type of respiratory function, as presented in Table 3, include respiratory rate, injection time, opening area, and total number of particles generated [7, 8, 29]. The particle size distributions generated by the four aforementioned respiratory activities are shown in Table 4 [7]. This study employs a discrete random walk (DRW) model [33]. When the number of particles is too low, the simulation results can be inaccurate. Due to the low number of aerosol particles for certain sizes, which can range from a few to dozens, coughing, sequential coughing, and speaking loudly are assumed to generate 10 times the number of particles to ensure a sufficient number for statistical analysis.

2.3. Numerical Model. The modeling of the elevator and human bodies was conducted using ANSYS SpaceClaim 2023, with mesh generation performed by the CFD preprocessing software Meshing. The continuous and discrete phase media within the elevator was computed using ANSYS Fluent 2023R1.

Only the air inlets and outlets of the elevator are activated initially, with human oral and nasal breathing disabled, to simulate the steady-state airflow field within the elevator. Once the flow field converges, the steady-state calculation data are used as initial values to activate the discrete phase model (DPM) for simulating the droplet transmission process. This study employs the unsteady Reynolds-averaged Navier–Stokes (RANS) equations, activates the energy equation, and utilizes the renormalization group (RNG) k-ε turbulence model [34] to calculate the velocity and temperature fields in the fluid domain. This turbulence model has been widely applied in airflow simulations of indoor spaces [24, 30]. For all flows, the laws of mass conservation and momentum conservation must be followed. The mass conservation equation can be written in the following form:

$$\frac{\partial \rho}{\partial t} + \nabla \bullet \left(\rho \vec{v} \right) = S_m. \tag{1}$$

In Equation (1), t represents time, ρ denotes the density of the continuous phase air, $\vec{v}$ represents the velocity of the continuous phase, and S_m is the mass added to the continuous phase from the dispersed secondary phase (e.g., due to droplet vaporization), as well as any user-defined sources.

The momentum conservation equation is as follows:

$$\frac{\partial}{\partial t}\left(\rho \vec{v} \right) + \nabla \bullet \left(\rho \vec{v} \vec{v} \right) = -\nabla p + \nabla \bullet \left(\bar{\bar{\tau}} \right) + \rho \vec{g} + \vec{F} \tag{2}$$

TABLE 2: Boundary conditions for all cases using oral and nasal breathing.

Boundary surface	Type	Velocity	Temperature	Relative humidity	Discrete phase boundary condition type
Inlet	Velocity inlet	20 ACH (0.126 m/s)	27°C	50%	Reflect
Outlet	Outflow	—	—	—	Escape
Mouth1 (source)	Velocity inlet	UDF1	35.5°C [28]	75% [29]	Reflect
Mouth2 (exposed)	Velocity inlet/wall	UDF2/no slip	33.5°C/31°C	75%/—	Escape/trap
Nose1 (source)	Velocity inlet	UDF3	35.5°C [28]	75%	Reflect
Nose2 (exposed)	Wall/velocity inlet	No slip/UDF3	31°C/33.5°C	—/75%	Trap/escape
Body	Wall	No slip	31°C, convective heat power 24 W [17]	—	Trap
Elevator walls/door/ceiling	Wall	No slip	Adiabatic	—	Trap

where p is the static pressure of the continuous phase, $\bar{\bar{\tau}}$ is the stress tensor, and $\rho\vec{g}$ and $\vec{F}$ represent gravity and external forces, respectively.

The turbulent kinetic energy k and its dissipation rate ε in the RNG k-ε turbulence model are obtained from the following transport equations:

$$\frac{\partial}{\partial t}(\rho\varnothing) + \frac{\partial}{\partial x_k}(\rho\varnothing v_k) = \frac{\partial}{\partial x_k}\left(\Gamma_{\varnothing,eff}\frac{\partial\varnothing}{\partial x_k}\right) + S_\varnothing \quad (3)$$

where $\varnothing$ is the scalar variable to be solved, including mass, velocity, temperature, energy, and turbulence variables. x_k and v_k represent spatial positions and velocities in three different directions, and $\Gamma_{\varnothing,eff}$ symbolizes the diffusion term in the equation, while $S_\varnothing$ represents the source term of the fluid. The finite volume method is used to solve the control equations within discrete elements. The SIMPLE scheme is employed for solving the Navier–Stokes equations through pressure–velocity coupling. The viscous term in the governing equations is discretized using a second-order central difference scheme, while the convective term is discretized using a second-order upwind scheme. Considering the temperature difference between the human body and the environment, the Boussinesq model is adopted for air density. When the residuals of velocity, continuity, turbulent kinetic energy, epsilon, and h_2o are all less than 10^{-4}, the equations are considered to be converged.

The temperature and velocity data of the airflow field, stabilized after simulation, are used as the initial conditions for the transient simulation. The transient simulation requires the activation of respiratory boundaries on the human model and the DPM [35]. The time step was set to 0.01 s; however, within the first 2 s of the simulation, the time step was set to 0.001 s to capture the peak velocities in the cough and sneeze airflow. The motion trajectories of the particles can be captured by the Lagrangian method in the DPM model, which allows for the individual tracking of all discrete phases and considers the influence of the continuous phase on the discrete phase. The maximum tracking step length was set to 5×10^7 to prevent particles that have not escaped within 2 min from not being tracked. Particles deemed trapped upon reaching surfaces like walls would have their trajectory tracking stopped.

After droplets and moist air are expelled from the mouth, the droplet cloud interacts with the surrounding air and gradually equilibrates to the ambient temperature. However, as long as there is evaporation of the droplet's volatile components, the temperature of the droplet will continue to decrease to the wet-bulb temperature. The driving force for evaporation comes from the difference in vapor pressure between the droplet surface and the water vapor in the air [33]. In the DPM model, the temperature-dependent latent heat is enabled, and aerosols are required to contain 1.8% solid matter as droplet nuclei. The evaporation equation and the droplet temperature conservation law are as follows:

$$S_v = ak_{mt}\left(\frac{P_{sat}}{RT_d} - X\frac{P}{RT}\right) \quad (4)$$

$$Nu = 2.0 + 0.6\,\mathrm{Re}_d^{0.5}Sc^{0.33} \quad (5)$$

$$\mathrm{Re}_d = \frac{\mu}{\rho d} \quad (6)$$

$$m_d C_{p,d}\frac{dT_d}{dt} = ha(T - T_d) + \frac{dm_d}{dt}h_{fg} \quad (7)$$

where S_v is the saturated vapor pressure, P_{sat} represents the air's saturation pressure, Nu is the Nusselt number, Re_d is the droplet's characteristic Reynolds number, m_d denotes the droplet mass, $C_{p,d}$ is the specific heat capacity at constant pressure, T and T_d represent the surrounding air and droplet temperatures, respectively, and h_{fg} is the latent heat of evaporation of the droplet. The evaporation rate of droplets is related to the diffusion gradient produced by the vapor pressure equilibrium on the droplet surface which can be expressed as

$$\dot{N} = k_c\left(C_{s,p} - C_{s,a}\right) \quad (8)$$

where k_c represents the heat and mass transfer coefficient, $C_{s,p}$ is the vapor concentration at the water droplet surface, and $C_{s,a}$ is the vapor concentration in the air.

Given that the particle sizes in this study were above the micron level, Saffman lift force is ignored. Due to higher density for the discrete phase (water) compared to the continuous phase (air), the virtual mass force and pressure

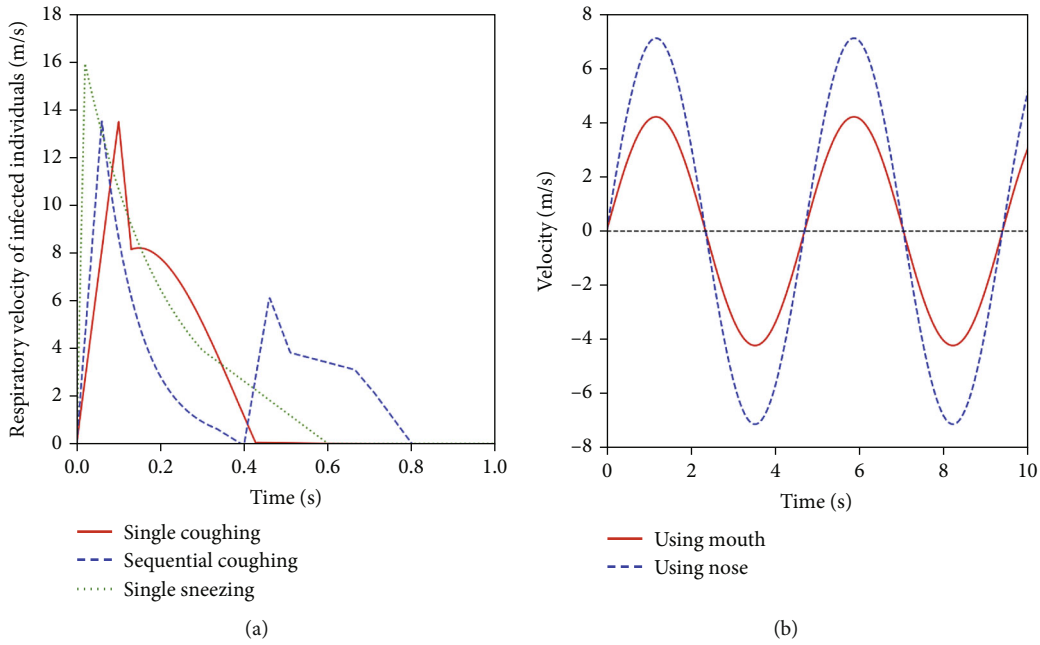

FIGURE 2: Respiratory velocity of (a) infected individual (source) under different respiratory behaviors (single coughing, sneezing, and sequential coughing) and (b) exposed individual using the mouth and nose.

TABLE 3: Boundary conditions for different respiratory patterns of infected individual (source) (refer to Table 1, V).

Respiratory process	Coughing	Sneezing	Speak loudly	Sequential coughing
Flow rate	Figure 4a	Figure 4a	1.11 m/s [30]	Figure 4a
Opening area	4 cm^2 [31]	1.3 cm^2 [32]	1.8 cm^2 [30]	4 cm^2 [31]
Droplet no.	5000/cough	1,000,000/sneeze	250/s	5000/cough

TABLE 4: Particle size distributions generated by four respiratory activities.

Diameter (μm)	Coughing	Sneezing	Speaking loudly	Sequential coughing
1.5	41	26,000	1	82
3	235	160,000	13	470
6	778	350,000	52	1556
12	1278	280,000	78	2555
20	700	97,000	40	1400
27.5	339	37,000	24	678
36	192	17,000	12	384
45	116	9000	6	232
60	76	5000	6	151
67	70	5000	5	140
87.5	49	4500	5	98
110	41	2500	4	82
137.5	31	1800	3	61
175	31	2000	2	61
225	27	1400	1	53
380	22	2100	3	45
750	12	1000	1	25
1500	4	140	0	8

gradient force are also disregarded. Furthermore, due to the small overall volume ratio of particles to the elevator's volume in this study, stochastic collision between particles is ignored. The motion model of the particles can be represented by the following equation:

$$\frac{dv_{p,i}}{dt} = \frac{F_M}{\tau_p}\left(v_{a,i} - v_{p,i}\right) + F_{p,i}. \tag{9}$$

The term $v_{p,i}$ represents the particle velocity in the i-direction. F_M denotes the drag correction function [36], which, along with the velocity difference between the discrete and continuous phases, constitutes the drag experienced by the discrete phase. $F_{p,i}$ represents the buoyancy term, related to the density difference between the two phases, equating to $g(\rho_p - \rho_a)/\rho_p$. τ_p is the characteristic response time of the continuous phase, calculated as $\rho_p D_p^2 C_c/18\mu_a$, where μ_a is the air viscosity, ρ_p is the density of the discrete phase, D_p is the particle diameter, and C_c represents the Cunningham slip correction factor, which can be expressed as

$$C_c = 1 + \frac{2\bar{\lambda}}{D_p}\left(1.257 + 0.4 * \exp\left(-\frac{1.1D_p}{2\bar{\lambda}}\right)\right) \tag{10}$$

where $\bar{\lambda}$ represents the mean free path of molecules. This method is known as the Stokes–Cunningham drag law, used to address discontinuity effects in the motion calculation of submicron particles. For large aerosol Reynolds numbers, a dynamic drag law is employed, assuming the droplet remains spherical throughout the domain. The correction factor is defined as

$$C_{d,\text{sphere}} = \begin{cases} 0.424 & \text{Re} > 1000, \\ \dfrac{24}{\text{Re}}\left(1 + \dfrac{1}{6}\,\text{Re}^{2/3}\right) & \text{Re} \le 1000. \end{cases} \tag{11}$$

The characteristic Reynolds numbers of the particles ranging from 1.5 to 1500 μm in the aforementioned motion do not exceed 1000, satisfying the conditions for using this method.

The mesh size near the human body surface was refined to 0.04 m, with grids at the mouth and nose created with a precision of 0.002 m. The mesh sizes at the air inlets and outlets were set to 0.005 m, while other mesh sizes were established at 0.05 m, utilizing tetrahedral mesh elements. A total of 3 million elements were generated. Figure 3 shows the mesh distribution inside the elevator and near the mouth and nose of the human model.

To verify mesh independence, this study established three different grid cell numbers, comprising a coarse mesh (1.5 million), a medium mesh (3 million), and a fine mesh (6 million). Figure 1a shows the reference line positions used for validation, with Line 1 ($Y = 1$ m) located at the center of the elevator and perpendicular to the horizontal plane between the two human models (X-Y plane), and Line 2 ($Z = 1.58$ m) aligned horizontally with the mouth of the human model, perpendicular to the Y-Z plane, with sampling every 0.01 m. This study selected the flow field 0.2 s after an infected individual coughs from the base case for comparison. Figure 4a,b compares the velocity and temperature values on the reference lines under different mesh sizes, with samples taken every 0.01 m. The results show slight differences among various mesh sizes but they were overall similar, with the error between the medium and refined meshes not exceeding 5%. Therefore, the medium mesh was chosen for further study.

2.4. Virus Load, Exposure Model, and Infection Probability Model. SAR-CoV-2 has been confirmed to exist in nasopharyngeal secretions, and during the early stages of infection, the viral content in saliva remains consistently elevated [37]. According to virological study [38], the viral load of SARS-CoV-2 in saliva often exhibits significant variations, with a median initial viral load typically around 10^7 copies/mL. In some cases, peak viral loads reach $10^{9.3}$ copies/mL or even up to 10^{11} copies/mL. Additionally, there is a significant correlation between viral load and the severity of the disease. To account for potentially more dangerous scenarios, the baseline viral load in droplets is set at 10^9 copies/mL. According to Anand et al. [39], the viral load carried by particles of different diameters varies, and the viral load for all particles must be multiplied by the respective fraction.

Currently, there is not sufficient evidence to confirm the exact dosage required to infect individuals with COVID-19. Exposure to small amounts of the virus is unlikely to cause infection, and the susceptibility may vary based on individual immune system strength. Official agencies and some research scholars have proposed a median infectious dose of 10–1000 viruses based on experimental studies [40]. Combining nasal pharyngeal CFD simulations and infection event estimates, 300 is the highest estimated value for the infectious dose. Based on probabilistic modeling of five large-scale transmission events, the viral dose causing infection is also estimated to be around 300–2000 copies [41]. Reports from the US Department of Homeland Security (DHS) indicated that SARS-CoV-2 infection may occur with 500 copies of the wild-type virus, 300 copies of the Delta variant, and 100 copies of the Omicron variant [42]. This study will use DHS data as a reference for infection dose to compare the impact of different variants on infection risk.

The Wells–Riley equation (Equation (9)) is often used as a simple and quick evaluation method for airborne infection risk [35] as it can reveal the infectivity, the intensity of the source of infection, the biological decay of the pathogen, etc. with specific quantitative indicators:

$$P(x, y, z, t) = 1 - e^{-Iqpt(1-\eta_l)(1-\eta_s)/Q} \tag{12}$$

where P is the probability of infection; I is the number of infectors; p is the pulmonary ventilation rate of susceptible people (meters cubed/hour); Q is the room ventilation rate (meters cubed/hour); q is the quantum generation rate by an infected person (h^{-1}); t is the exposure time (hour), and η is the mask efficiency. However, the Wells–Riley equation has two major limitations: (i) the room air is assumed to be perfectly mixed such that the virion concentration is

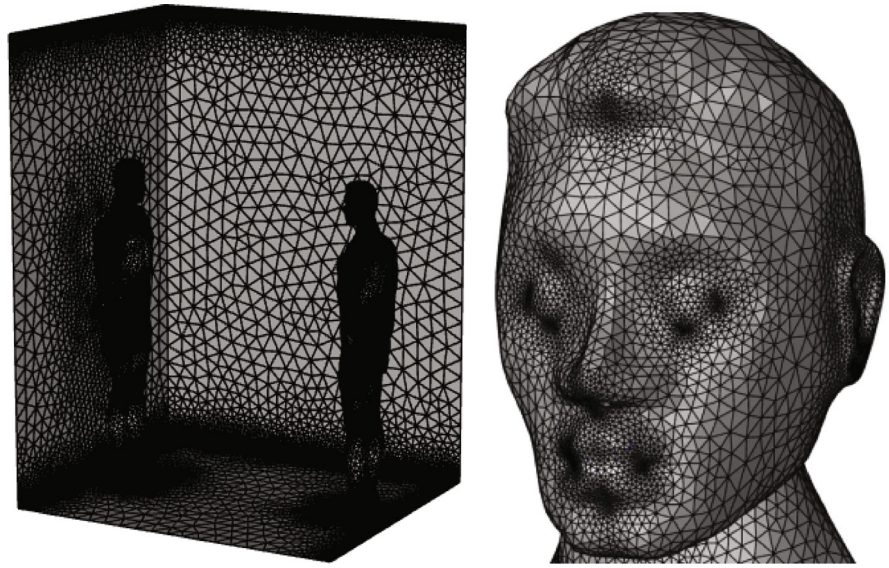

(a) (b)

FIGURE 3: Mesh distribution used in this study: (a) inside the elevator and (b) near the mouth and nose of the human model.

uniformly distributed in the space, and (ii) the equation neglects the viability and infectivity of the pathogen quanta. To overcome these limitations, a modified stochastic dose–response model [43] is proposed in this study to estimate the probability of infection, represented by the following equation:

$$P(x, y, z, t) = 1 - e^{-d/ID} \tag{13}$$

where ID represents the infectious dose of the virus; d is the accumulated viral dose at location (x, y, z) due to inhalation of droplet particles over exposure time t, and d can be calculated as

$$d = Q_E r \int_0^{t_0} \left\{ \sum_{m=1}^{n} q_m(x, y, z, t) \beta_m \left(1 - \eta_{S,m}\right) \frac{\pi (D_m(x, y, z, t))^3}{6 S_m^3} \right\} f(t) dt \tag{14}$$

where Q_E represents the inhalation rate of the exposed individual (cubic meters per hour); r is the inhalation rate of the exposed individual (meters cubed/hour); n is the number of size categories of inhaled droplets; q_m is the local concentration value of the mth category of inhaled droplets (m^{-3}); m is the deposition rate of droplets in the nasopharynx related to the diameter of inhaled droplets; β_m is the filtration coefficient of the nasopharynx, which is a function of the diameter of the inhaled droplets [40]; η_{sm} is the mask filtration efficiency of the exposed individual; D is the initial diameter of respiratory droplets (meter); S_m is the shrinkage rate due to evaporation of emitted droplets during transmission; $f(t)$ is the survival rate or survival function of pathogens in aerosols; and t is the exposure time of the susceptible individual.

The CFD simulation used can accurately track the movement of each droplet, and Q_E and $q_m(x, y, z, t)$ can be converted into the number of droplets inhaled by the exposed individual. $P_m(t_0)$ can reduce the complexity in collecting viral concentration distribution data, while $q_m(x, y, z, t)$ can minimize the impact on the accuracy of the results. The simplified model is as follows:

$$d = c \sum_{m=1}^{n} P_m(t_0) \frac{\pi (D_I(x, y, z, 0))^3}{6}. \tag{15}$$

$P_m(x, y, z, t)$ represents the number of virus particles inhaled by exposed individuals, which can be directly obtained from CFD simulations. $D_I(x, y, z, 0)$ represents the initial diameter of inhaled particles, which is set before CFD simulations. The diameter of particles after evaporation can be obtained from CFD simulations. Note that the amount of virus carried by a single droplet is calculated from the initial volume at the time of release, and the droplet deposition rate in the respiratory tract is determined by the diameter of the evaporated droplet core inhaled by the exposed person. $f(t)$ denotes the virus survival rate at time t. Since the duration from virus inhalation initiation to completion of human inhalation (passage of the virus cloud past the human body) is relatively short in CFD simulations (on the order of seconds), $f(t) = 1$.

3. Results and Discussion

3.1. Validation. To ensure the accuracy of the CFD model used for particle transport simulation in this study, comparisons with experimental data were conducted to validate the continuous phase velocity field, evaporation model, and particle dispersion model. This study employed experimental data from Chao et al. [8] to validate the evaporation model, particle size dispersion ratio, and particle diffusion model. The computational domain was an indoor space with dimensions of 4.8 m (length) × 4.8 m (width) × 2.6 m

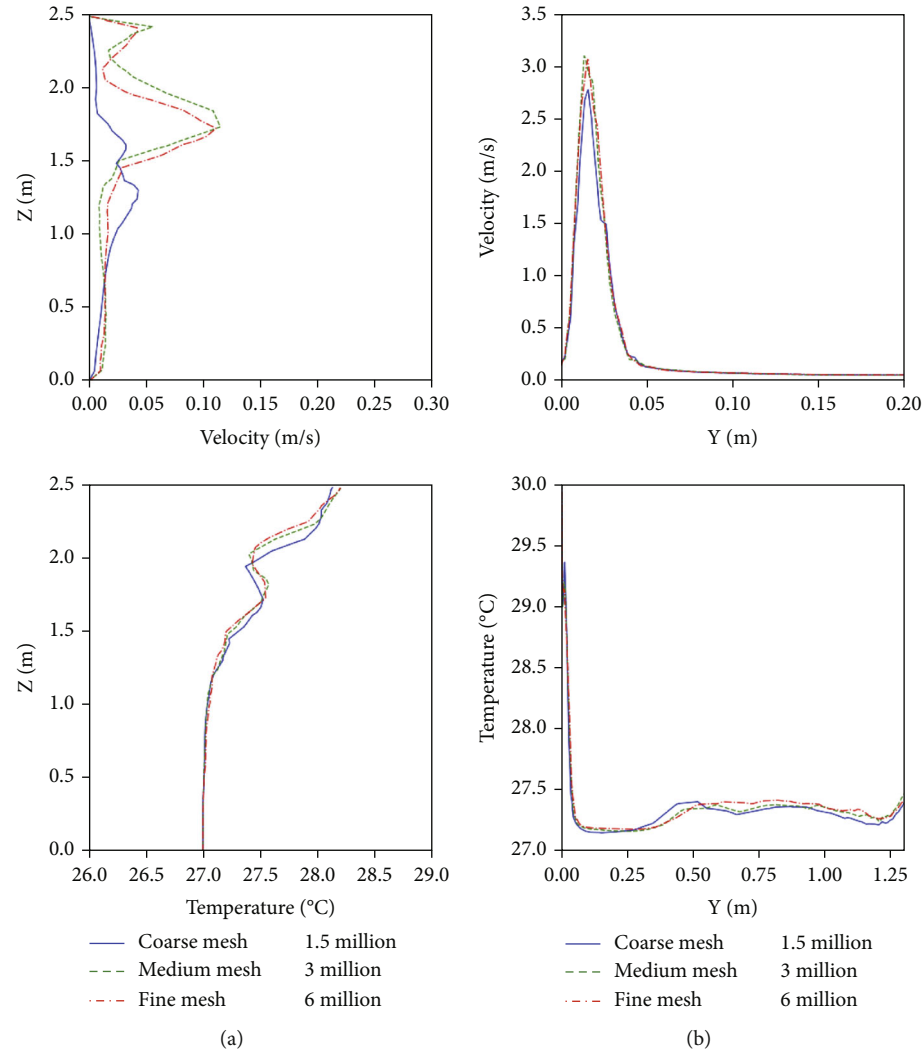

Figure 4: Comparison of the air velocity and air temperature with different mesh at location: (a) $Y = 1$ m; (b) $Z = 1.58$ m.

(height), featuring unidirectional downward flow. The top serves as the velocity inlet, supplying air at velocity of 0.1 m/s with temperature of 20°C and relative humidity of 55%. The bottom is used as the air outlet, as illustrated in Figure 5a. Particle clusters are injected at the center of the room, 0.8 m above the ground, consisting of evaporating water droplets (with a vaporization fraction of 0.982), injected at a velocity of 10 m/s in the vertical upward direction, at a temperature of 307 K. Figures 5b, 5c, and 5d show the variation of the particle size of the discrete phase over time, the variation of the vertical position of the discrete phase in unidirectional downward flow, and the variation of the mean square displacement of the horizontal position of the discrete phase. Mean square displacement can be expressed as follows:

$$\text{Mean square displacement} = \frac{\sum_{i=1}^{n}[x_i(t) - x_i(t_0)]^2}{n} \quad (16)$$

where $x_i(t_0)$ represents the initial x position of the droplet when it is ejected from the nozzle, $x_i(t)$ represents the x position of the droplet after t seconds of injection, and n represents the total number of droplets injected.

The comparative results indicate that differences are below 5%, affirming the validity of the evaporation model and the DPM particle diffusion model.

3.2. Impact of Ventilation OP. The position of the elevator ventilation outlet will firstly be conducted to assess their impact on the spread of virus particles. The majority of existing elevators adopt a design with exhaust vents located at the bottom, but there are few designed with exhaust fans at the top. Figure 6 shows the distribution of virus-carrying particles in the elevator at different exhaust positions at the 120th second after the infected person coughed. It can be observed that as the exhaust vent moves upward, the number of airborne particles increases significantly, and particles that would normally settle are also found floating in the air. When the exhaust vent is positioned at the top, more particles are concentrated near the top of the elevator and in the breathing zone of individuals. Since the exhaust is at the top, the upward airflow in the elevator is strongest, carrying

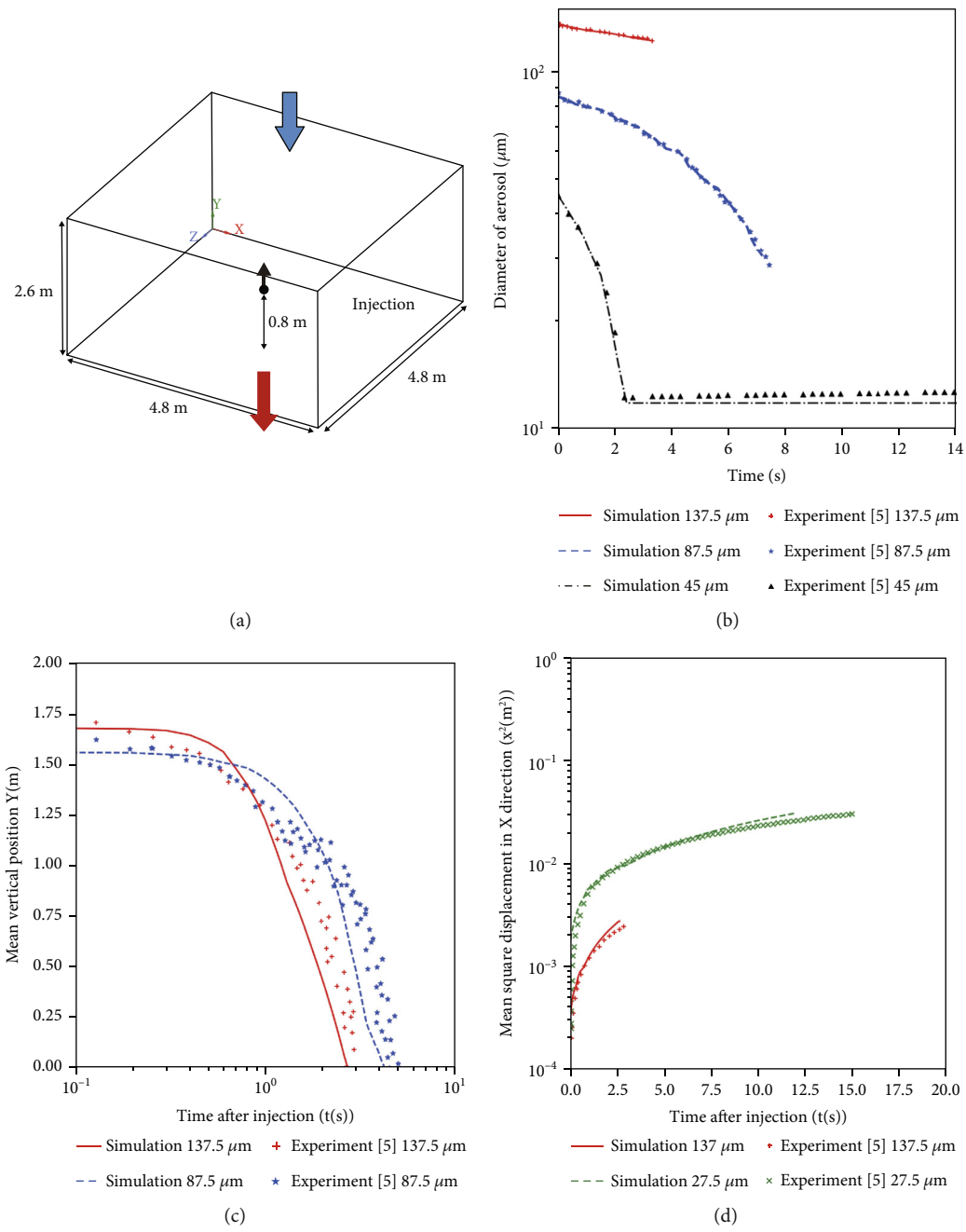

FIGURE 5: (a) Computational model, (b) variation of the particle size of the discrete phase over time, (c) the variation of the vertical position of the particle in unidirectional downward flow, and (d) and the variation of the square difference of the horizontal position of the particle.

more particles into the breathing zone, thereby increasing the risk of exposure to more viruses.

Figure 7 presents histograms of particle distribution inside the elevator with different ventilation outlet locations at 120 s. There are four positions for particles in elevators: suspended in air, attached to elevator floors or walls (trapped), escaping from the elevator through ventilation exits (escaped), and being inhaled into the respiratory tract by the exposed individual (inhaled). It can be seen that the particles inhaled by the exposed individuals only account for a small fraction of the released particles, not exceeding 2%. Regardless of the breathing pattern, the most effective particle removal occurs when the outlet is located in the middle of the elevator. This is because when vents are positioned in the middle, the distance travelled from the infected individual to the vents is the shortest. However, this does not imply that individuals inside the elevator are the safest, as most of the particle removal path passes through the breathing zone of the occupants. When the exhaust is located at the bottom, particle removal is less effective, with about 80% of particles remaining airborne. The ventilation system only expels about 10% of the particles, but this method results in the highest particle deposition compared to the other three methods. Assessing the risk of virus transmission

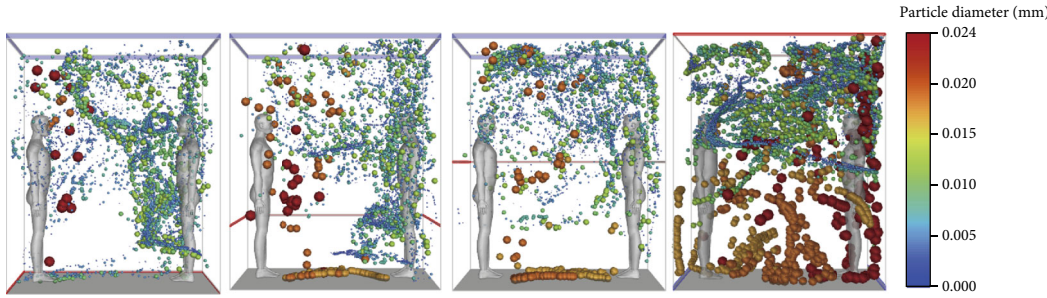

FIGURE 6: Distribution of virus-laden particles inside the elevator at 120 s after the infected person coughed for various ventilation outlet positions (left: infection source, right: exposed individuals, subsequent diagrams follow this layout unless noted otherwise).

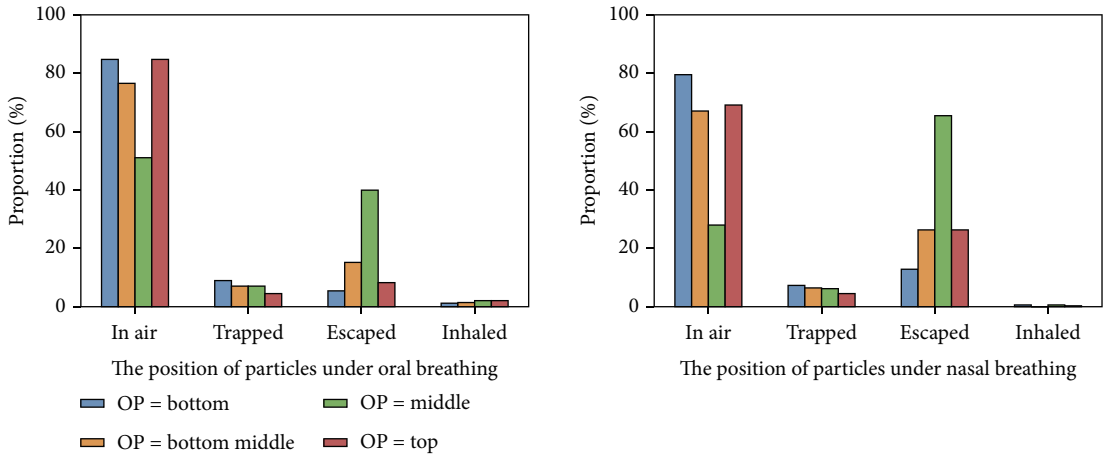

FIGURE 7: Histograms of position distribution of particles inside elevator at 120 s under different ventilation outlet positions (OPs).

inside elevators requires considering the amount of virus inhaled by individual during the ride, rather than relying solely on the purification efficiency of the ventilation system for particles.

The cumulative virus inhalation dose over time for individual breathing through the mouth and nose of the exposed person is shown in Figure 8. The results show that using top outlet poses the greatest risk, as individual inhales particles first, with the highest cumulative intake. The use of middle outlet also results in close virus inhalation amounts, supporting the aforementioned findings. Employing bottom outlet has been proven to be the safest approach, with individuals inhaling the virus last and accumulating the least amount of particles during the brief elevator ride. When using bottom exhaust ventilation, virus-laden particles are initially released from the infected person's mouth and are carried to the chest and abdomen of the exposed person due to downward airflow from the ventilation system and gravity. They then rise to the breathing zone due to buoyancy effects from upward thermal plumes, leading to inhalation. With middle or top exhausts, particles are transported more quickly to the breathing zone by stronger upward airflow from the ventilation system. The study also found that particle inhalation exhibited a gradient increase, with the initial inhalation (corresponding to the first gradient increase in Figure 8) involving a higher viral dose compared to subsequent inhalations. When the particle cloud first reaches the breathing zone of the exposed individual, it is less influenced by the body's thermal plume and remains more concentrated. Over time, the combined effects of the rising thermal plume, the exposed individual's breathing airflow, and ventilation airflow cause the particle cloud to gradually disperse, reducing its concentration. Consequently, subsequent inhalations result in progressively lower viral doses (corresponding to the later gradient increases in Figure 8).

Finally, this study quantified the infection probability of exposed individuals after a 2-min elevator ride based on the virus inhalation dose and the infectious dose of several viral strains, with the viral load of SARS-CoV-2 in particles fixed at 10^9 copies/mL. As shown in Figure 9, using bottom outlet as the safest approach, infection probabilities for exposed individuals are found to be below 40% for all strains except the Omicron variant. Additionally, infection probabilities slightly increase with higher exhaust positions because particles are more likely to enter the breathing zone. However, since the particles inhaled are often larger and filtered out by the respiratory tract [40], the infection risk is not significantly higher compared to a bottom exhaust. This demonstrates that the widely adopted bottom outlet ventilation method is safer and promotes the faster settling of particles.

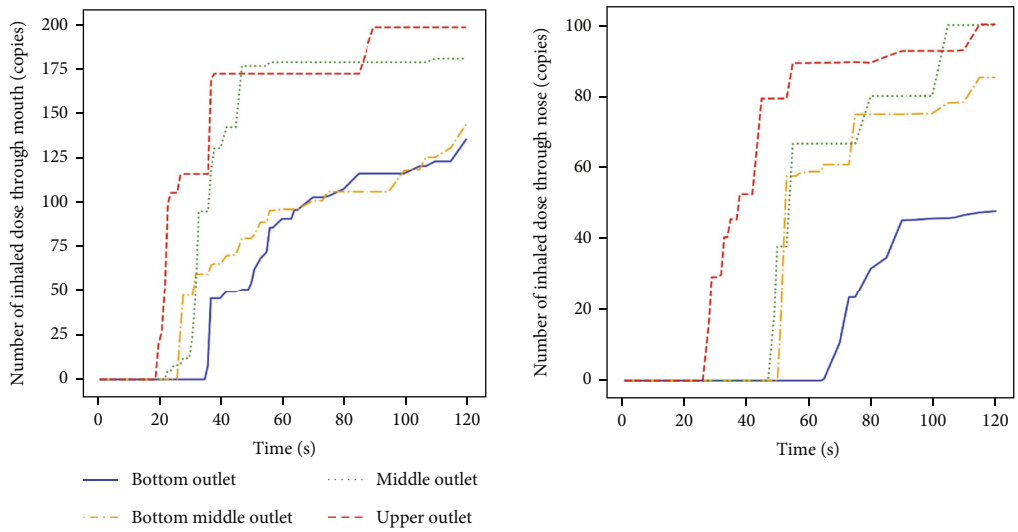

FIGURE 8: Cumulative virus inhalation of individual exposed to oral and nasal breathing over time under different ventilation outlet positions (OPs).

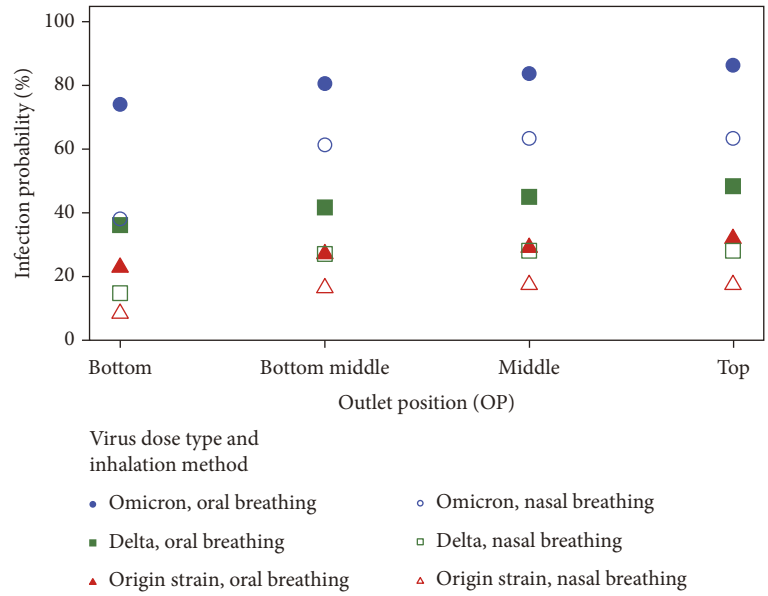

FIGURE 9: Analysis of infection probability of exposed individual under different ventilation outlet positions (OPs).

This is consistent with the findings of Liu et al. [44] and Li et al. [24], who similarly argue that bottom-inlet, top-outlet DV is more hazardous. This study suggests that exhaust position, purification time, and human breathing patterns can all affect the transmission risk of SARS-CoV-2 in elevators.

3.3. Impact of Ventilation Volume. Our study examined the impact of different ventilation rates on virus transmission, covering six scenarios from ACH = 3 to 72.

This section presents the results for Cases 9–10. The amount of air entering the elevator may vary depending on the performance of the ventilation system. ACH = 3 indicates nonfunctioning air conditioning, with the elevator in a stagnant state, while ACH = 72 represents air conditioning equivalent to the minimum airflow required for 16 people breathing in a 3-m^2 space. Figure 10 shows the distribution of virus-laden particles in the elevator at different ventilation volumes at 120 s after the infected person coughs. At lower ventilation rates, the downward airflow from the ventilation system is weaker than the upward thermal plumes near the human body. As a result, particles located around the chest area of a person rise and accumulate around the passenger's head. This demonstrates that the ventilation system's ability to remove particles is inadequate at lower ventilation rates. However, as ACH increases to 50, suspended particles in the air significantly decrease and become more evenly distributed. The maximum diameter of suspended particles decreases from 0.0238 to 0.0122 mm, indicating that higher

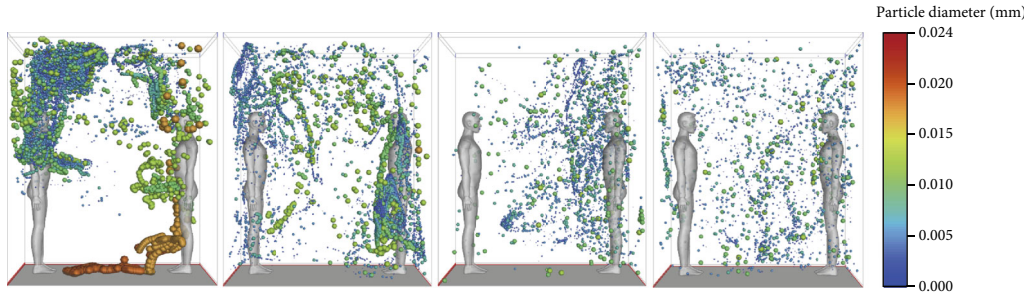

(a) ACH = 3 (b) ACH = 30 (c) ACH = 50 (d) ACH = 72

FIGURE 10: Distribution of virus-laden particles inside the elevator at 120 s after the infected person coughs at different ventilation volumes.

ventilation rates accelerate the deposition of larger particles and expedite their expulsion.

The particle distribution inside the elevator varies under different ventilation rates. The particle distribution histogram at 120 s after coughing of the infected person, as shown in Figure A2a in Appendix II, shows that a significant increase in particle expulsion efficiency with higher ventilation rates. At $t = 120$ s and ACH = 30, 40% of the particles have escaped from the outlet, which is consistent with Nirvik's study [21]. Similarly, this effect can be achieved at $t = 120$ s with ACH = 30. When the air conditioning is turned off at ACH = 3, the total number of particles inhaled by the exposed person also does not exceed 2%. Slight airflow disturbances have a more significant impact on small particles. Switching passengers to nasal breathing can greatly reduce the risk of inhaling viruses, as nasal breathing causes the inhaled air direction to form a larger angle with the particle cloud direction, leading to airflow deflection and reduced particle intake. Mouth breathing, however, provides a more direct and smoother airflow path. Additionally, the nasal breathing area is significantly smaller than the mouth breathing area, which further reduces the risk of particle inhalation.

Under different ventilation rates, there will also be significant differences in the cumulative amount of virus inhaled by exposed individuals over time. As time increases, the cumulative dose in all cases continues to rise. This is because many particles initially disperse upwards before gradually descending into the occupants' breathing zone. As ACH increases, the cumulative dose gradually decreases. At 30 ACH, the cumulative intake for the exposed is sufficiently low. This phenomenon is also validated by Liu et al. [25], but it only analyzed nasal breathing and did not specifically address the particle size distribution of inhaled particles. When using nasal breathing, the start time of inhaling virus particles is significantly later than mouth breathing, further proving the safety of nasal breathing. More details can be found in Figure A3a in Appendix III.

Figure 11 depicts the particle size distribution of the final inhaled particles under different ACH levels. It can be observed that the sizes of inhaled particles exhibit some randomness, but all fall within the range of 45 μm and below. The virus content carried by particles increases with the increase in particle size. As ACH increases, the proportion of inhaled fine particulate matter begins to increase. When the ventilation rate reaches ACH = 30, the diameter of the particles inhaled by the exposed person is already less than 30 microns, with larger particles having already settled to the ground under the effects of downward airflow.

Regarding the analysis of infection probability at different ACH levels, the viral load of particles is fixed at 10^9 copies/mL. Although higher ACH levels result in a higher proportion of small particles being inhaled, the total number of inhaled particles is much lower compared to low ACH levels. This results in a higher infection risk at lower ACH levels. At ACH levels of 3 and 10, the probability of the exposed individual inhaling the Omicron strain through mouth breathing is 96% and 94%, respectively. As ACH increases, the probability of infection with various virus strains decreases. Furthermore, nasal breathing is found to be safer than mouth breathing. When ACH = 30, the probability of infection through nasal breathing is already very low, less than 5%.

However, when ACH = 50, the likelihood of infection through oral breathing reaches a similar value. By normalizing the data, it can be found that the probability of infection does not seem to be affected by the type of virus when breathing through the nose, and the ventilation rate also changes. At ACH = 30, the infection probability has decreased to around 0.05 compared to ACH = 3, with a less pronounced decrease thereafter. Conversely, when breathing through the mouth, at ACH = 50, the infection probability has dropped to below 0.2 of the ACH = 3 level, with a similarly diminished subsequent decline. More details can be found in Figure A4a in Appendix IV. Increasing ventilation volume in ventilation systems typically correlates with higher power. Considering energy efficiency and recent studies [25], setting the elevator ventilation to around ACH = 30 appears to be an appropriate configuration. This setting corresponds to an airflow velocity of 0.188 m/s at the ventilation inlet, which is significantly lower than the airflow and energy consumption levels typical of household air conditioning systems [45].

3.4. Impact of Temperature and Relative Humidity. The atmospheric environment varies across different latitudes and longitudes, so it is essential to investigate the impact of varying temperatures and relative humidity on virus transmission. Figure 12 illustrates the particle distribution inside the elevator at 120 s after the infected person coughed under

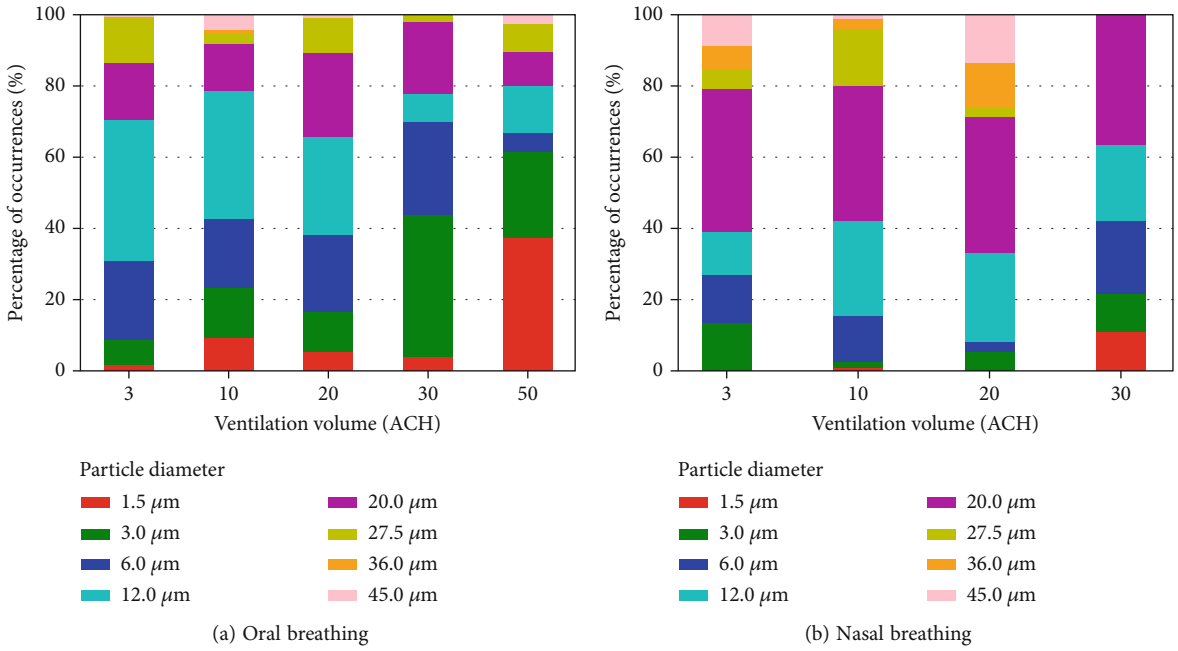

Figure 11: Particle size distribution of the final inhaled particles by exposed individual under different ACH.

different temperatures. Through Figure 12a,b, it can be observed that as the temperature increases, the rising thermal plume gradually weakens, leading to a stronger removal effect of particles. At lower temperatures, distinct vortices also form, but these vortices diminish the purifying capacity of the ventilation system. Moreover, the strong upward airflow can elevate the particle cloud to above the human breathing zone, resulting in a more uniform particle distribution within the breathing zone. At a temperature of 27°C (Figure 12c), a significant amount of particles accumulates in the breathing zone of occupants, posing greater risks. In addition, relative humidity variation mainly affects the evaporation rate of particles; as relative humidity increases, particle evaporation slows down, with the maximum diameter of suspended particles in the air being 0.0122 mm. This indicates that, compared to low relative humidity conditions, most particles would have settled on the ground.

Different temperatures and relative humidity can also affect the distribution of particles inside elevators. Figure 13 shows the histograms of particle position distribution under different temperatures and relative humidity. It can be observed that increasing temperature and relative humidity can slightly improve the purification capacity of the ventilation system, although this improvement is not significant and may affect human comfort. Regarding the cumulative virus inhaled by exposed individuals under different temperatures and relative humidity, the results in Figure A3b show that as the temperature rises, the amount of virus inhaled by the exposed individual gradually increases. When the temperature reaches 27°C, the cumulative viral inhalation of the exposed individuals peaks. However, once the environmental temperature rises to match body temperature, the cumulative inhalation amount for exposed individuals drops to zero. At lower temperatures, the buoyancy effect of thermal plumes near the body is stronger (Figure 12a,b). After an infected person coughs, the particle cloud experiences significant uplift and reaches the head region, where it then disperses downward with the airflow. In the 27°C base case (Figure 12c), the buoyancy effect of the thermal plume is not as pronounced as at lower temperatures; the particle cloud first reaches the chest and neck area of the exposed individuals due to the combined effects of the cough and ventilation airflow, before the upward buoyancy effect allows it to reach the breathing zone. When environmental temperatures exceed body temperature (Figure 12d,e), the buoyancy effect of thermal plumes becomes negligible compared to the downward airflow from the ventilation system, causing particulate matter to accumulate below the breathing zone of the exposed individuals, thus reducing the likelihood of inhaling the virus. This reveals that different temperatures have a significant impact on virus transmission, indicating an optimal transmission temperature. Additionally, it is noteworthy that an increase in relative humidity slightly reduces the viral load inhaled by exposed individuals, though the effect appears to be minimal.

Figure 14 presents the initial size distribution of particles ultimately inhaled under varying temperatures and humidity. Figure 14a shows conditions with a constant humidity of 50% and a changing temperature gradient, while Figure 14b shows conditions with a constant temperature of 27°C and varying humidity. It is observed that an increase in temperature results in a higher proportion of smaller diameter particles being inhaled by individuals, and a similar effect is achieved with increased relative humidity. This may be due to the fact that higher temperatures cause more small particles to remain suspended in the breathing zone of the exposed individual. Meanwhile, increased relative humidity reduces particle evaporation, leading to the settlement of larger diameter particles. The probability of infection under different temperatures and humidity, which is closely related to the number

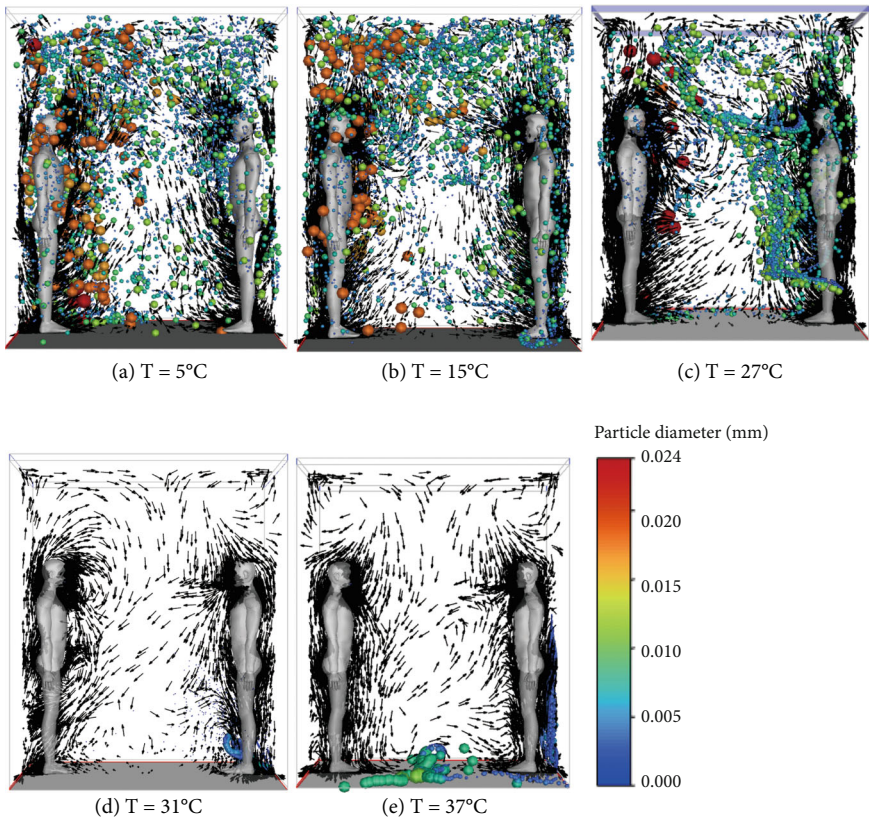

FIGURE 12: Distribution maps of virus-laden particles and velocity vector inside the elevator at 120 s after the infected person coughs at different temperatures (T).

of inhaled viruses and the infectious dose required to trigger an infection, is discussed. The results indicate that below the surface temperature of the human body, the probability of infection gradually increases with the rise in environmental temperature, as shown in Figure 15a. However, when the environmental temperature exceeds the human body surface temperature (31°C), the probability of infection for the exposed individual is nearly zero. Additionally, an increase in relative humidity can slightly reduce the probability of infection for the exposed individual, with 95% achieving the best effect in this study, as shown in Figure 15b. These results are consistent with the findings of Anice et al. [46] and Mao Wang et al. [47], who found that high temperature and humidity help reduce the risk of virus transmission. Specifically, when the temperature rises to 30°C and the relative humidity is at 35%, the probability of infection drops to zero. Similarly, Nirvik [21] has drawn comparable conclusions in studies conducted in indoor environments.

3.5. Impact of Ventilation Methods. This section examines the usage of elevators in densely populated areas of Hong Kong including the mainstream ventilation methods, which include side ventilation, central ACV, and distributed ACV. In elevators with side ventilation systems, droplets directly reach the breathing zone of exposed individuals in less than 30 s. In contrast, elevators with ACV systems exhibit a significant downward airflow directly beneath them, which initially acts as a protective curtain, accelerating the descent of particles. However, once droplets reach the vicinity of the exposed individual, they rise again through the upward flow induced by the thermal plume, passing through the breathing zone once more. Nevertheless, ACV does delay the time it takes for particles to reach the human breathing zone. Moreover, within 120 s, the distribution of contaminants inside the elevator is more uniform. The detailed information on the temporal distribution of particles in elevators under three ventilation methods can be found in Figure A1 in Appendix I.

The use of different elevator ventilation methods can also result in different particle distributions inside the elevator, as shown in Figure A2b. With constant ventilation volume, ACV improves particle clearance, and the effectiveness increases over time. Among them, the distributed ventilation system shows the best cleaning effect, with a threefold increase in efficiency compared to side ventilation systems. The proportion of particles inhaled by the exposed person under these three ventilation modes does not exceed 1%. Regarding the cumulative inhalation of viruses under different ventilation modes (Figure A3c), side ventilation remains the most dangerous, with the exposed individual inhaling the highest amount of virus. The amount of virus inhaled by an individual under the two ACV modes is similar. However, compared to central air curtains, individuals in an elevator ventilated with distributed air curtains inhale the virus later, indicating that distributed air curtains are safer for short elevator rides. Therefore, it can be concluded that the probability of infection for different

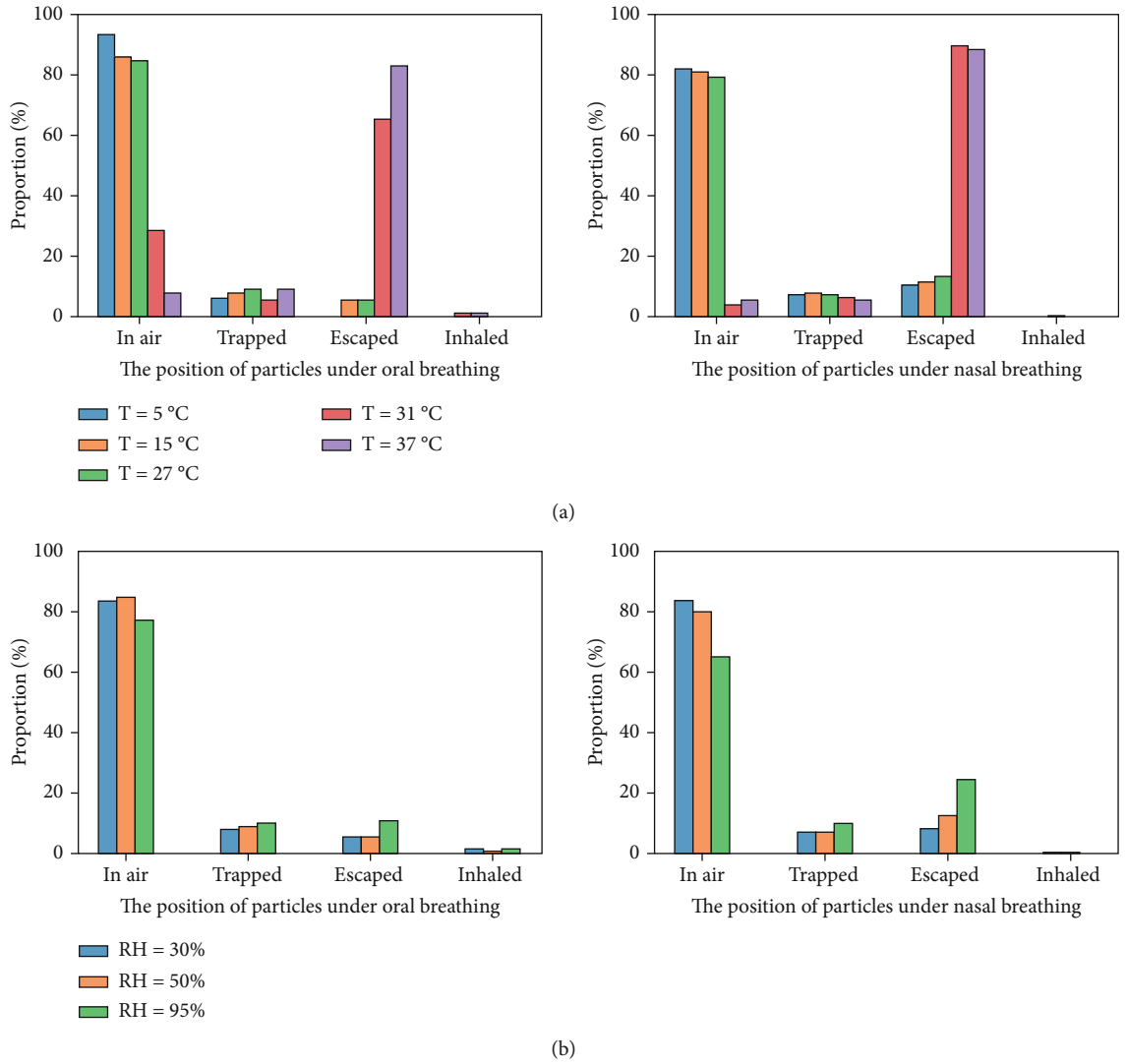

Figure 13: Histograms of position distribution of particles inside elevator at 120 s under different (a) temperatures (T) and (b) relative humidity (RH) of supplied air.

viruses varies among exposed individuals under different ventilation methods. Due to the relatively low ventilation rates of all three methods, which are set at 20, the probability of infection for individuals exposed to the Omicron variant exceeds 50%. Under the same conditions, individuals using side ventilation systems have an infection probability that is 5%~10% higher than those using the other two ventilation methods. The infection probabilities vary among different ventilation methods in an elevator, with ACV being safer, particularly distributed ventilation. Li et al. [24] reached similar conclusions through particle dispersion trajectory analysis, indicating that ACV is safer than conventional MV and DV (with lower inlet and upper exhaust). More detailed information regarding the impact of ventilation methods on the infection probability of exposed individuals can be found in Figure A4b.

3.6. Impact of RPs of Infected Individual. The section investigated the impact of various respiratory activities of the infected individual on the particle transmission of the virus. Sneezing generates a dense particle cloud that accumulates around the head and breathing zone of the exposed individual (Figure 16a). Conversely, particles emitted from speaking loudly, due to their lower initial velocity, primarily gather near the head of the infected individual under the influence of thermal plumes, with some particles being transported upwards toward the top of the elevator by horizontal airflow, albeit in limited quantities (Figure 16b). Both sequential coughing and a single cough result in particles initially reaching the vicinity of the exposed individual and then moving upwards to the top of the elevator under the influence of rising airflow before dispersing (Figure 16c). Furthermore, due to consistent ventilation modes and airflow rates, there is minimal variation in the proportional distribution of particles generated by different RPs.

Regarding the cumulative inhaled viral load by the exposed individual, sneezing by the infected individual results in a virus inhalation level 1–2 orders of magnitude higher than other RPs, and the virus inhalation by the

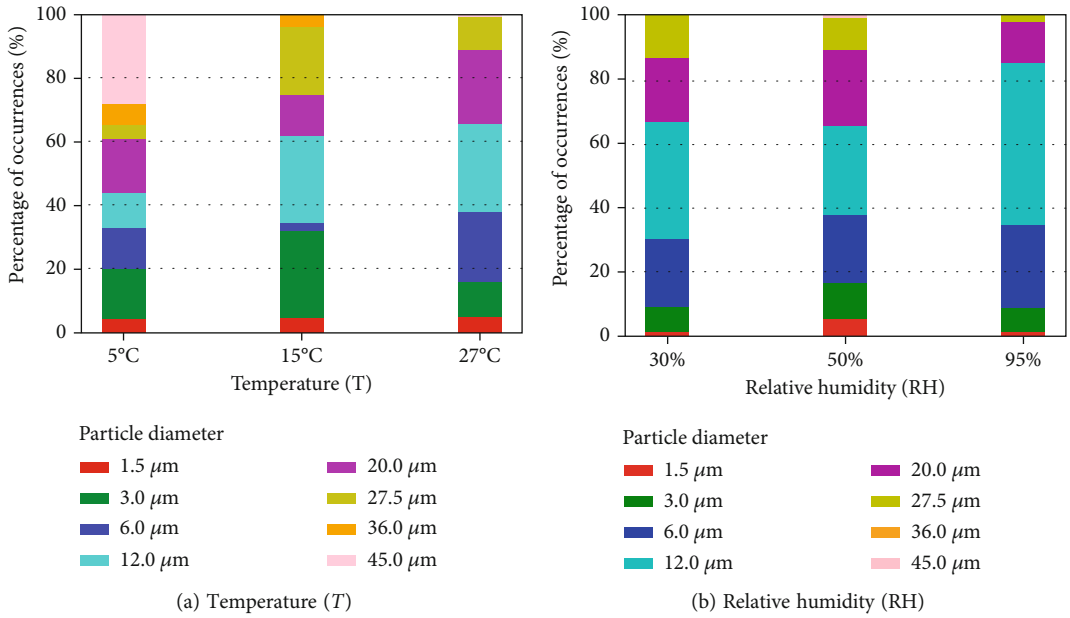

Figure 14: Particle size distribution of the final inhaled particles under different temperatures and relative humidity.

exposed individual occurs earlier than other methods. In cases of speaking loudly, the amount of viral copies inhaled by the exposed individual is very low, almost negligible. Conversely, in cases of sequential coughing, the number of viral copies inhaled is approximately six times higher compared to single coughing. When facing situations involving sneezing and multiple coughing, individuals in the same elevator compartment will face a higher risk. However, maintaining sufficient distance from the infected individual, the impact of speaking loudly and conversing during elevator rides can be considered negligible. More details about the results can be found in Figure A3d in the Appendix III.

According to the infection probability analysis, when the infected individual sneezes, the infection probability caused by all viral strains reaches 99%. In the case of sequential coughing, both the Omicron and Delta variants pose a significant threat. However, for speaking loudly, the infection probability caused by all viral strains remains below 20%.

3.7. Impact of Body Types Between Infected and Exposed Individuals. This section analyzed the impact of body type differences between the source and the exposed individual on the inhaled virus dose and infection probability. In reality, virus transmission varies among genders, adults and children, and among children themselves. Individuals of different heights and weights have varying rates and frequencies of breathing, as well as differences in the surface area of the mouth and nose through which they breathe, thereby affecting virus transmission. Figure 17 illustrates the distribution of particles in an elevator among passengers of different body types. It is observed that when the infected individual is an adult, particle clouds consistently exist within the breathing zone of those exposed, as shown in Figure 17a. The lower the height of the exposed individual, the more uneven the particle distribution, with a higher concentration in their breathing zone. This occurs because the particle cloud generated by an adult male's cough moves directly toward the face of an adult female (at the same chest height) due to downward airflow and gravity, as shown in Figure 17b. Additionally, once particles reach the breathing zone, they are influenced not only by thermal plumes but also by the respiratory airflow of the exposed individual. Since their breathing rate is less than that of an adult male, the outward momentum of the particles is lower, resulting in a more concentrated appearance rather than being dispersed. When the exposed individual is a child, the surrounding thermal plume is relatively weaker compared to that of an adult male (with a smaller thermal surface), resulting in less upward momentum from buoyancy effects, causing particles to gather in the child's breathing zone, as shown in Figure 17c. However, when the source is a child, most particle clusters tend to accumulate in the space near the infected individual, with only a small number reaching the breathing zone of the exposed individual, as shown in Figure 17d. Due to children's generally lower height and weight, the initial speed of particles produced by coughing is also lower, lacking the energy to carry the cloud of airflow to the exposed individual. Therefore, in cases where the source of infection is a child, variations in the height and body type of the exposed individual do not need to be considered. The findings of this study have been validated in previous research [48].

Regarding the analysis of infection probability (Figure A4d), the risk of infection for children and adult women is quite high, with infection probabilities close to 99%. This is because, in this case, the exposed person inhales more particles. In the case of two children facing each other,

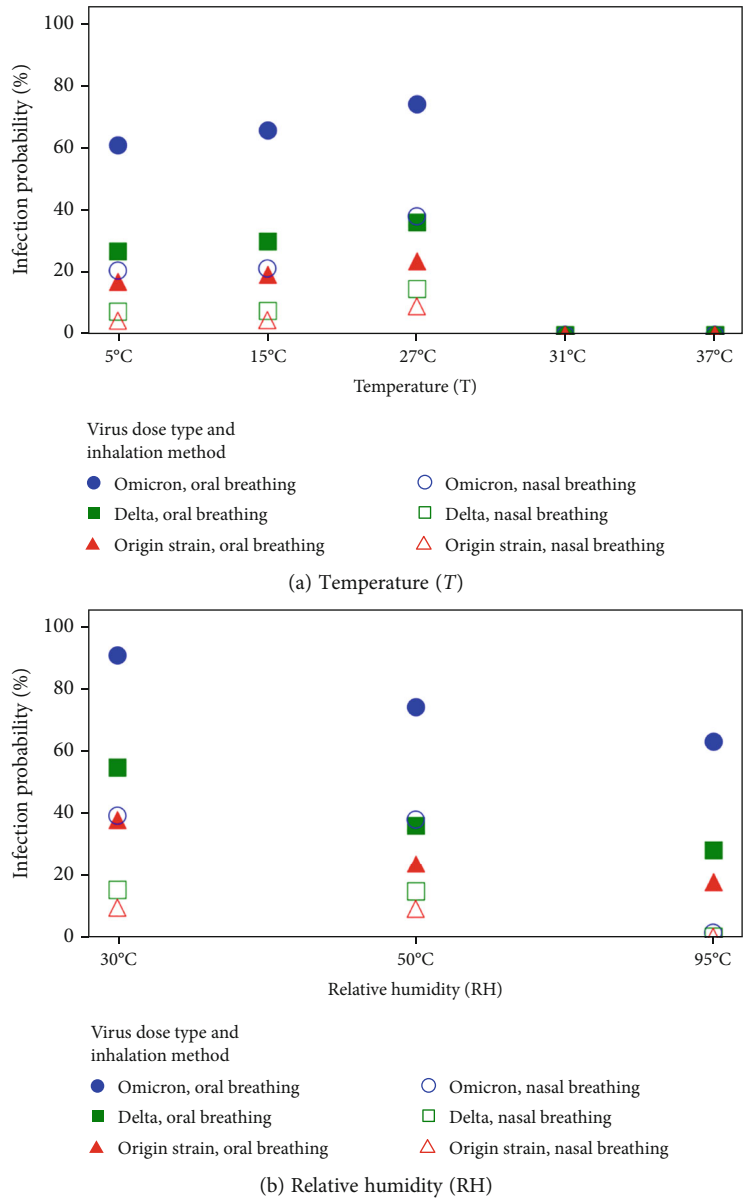

Figure 15: Analysis of infection probability of exposed individual under different temperatures and relative humidity.

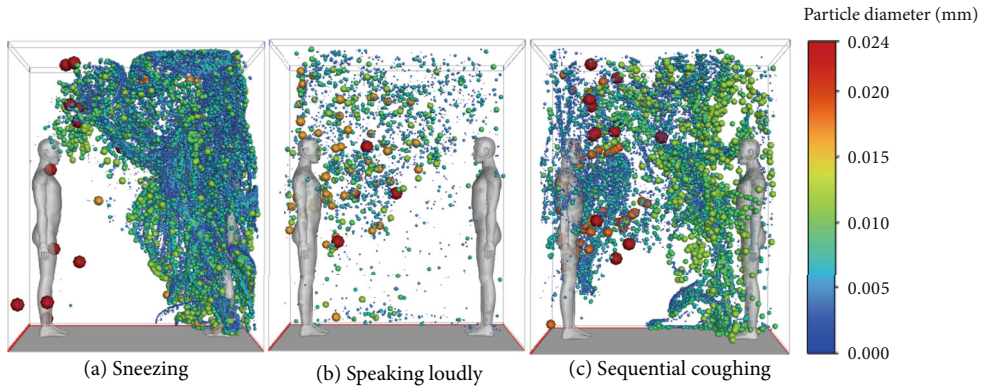

Figure 16: Distribution maps of virus-laden particles and velocity vector inside the elevator at 120 s after the infected person coughs at different temperatures (T).

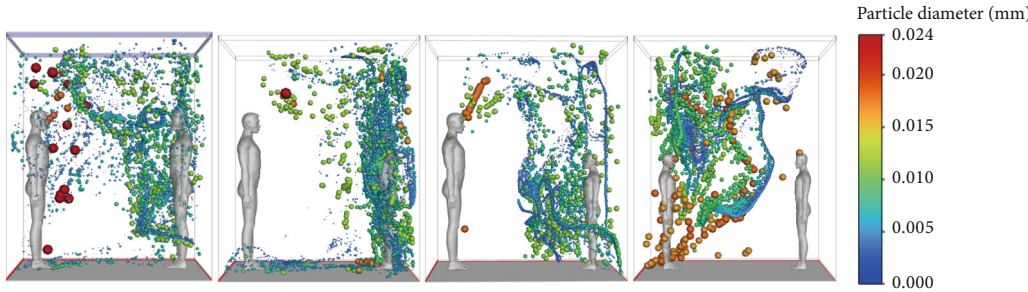

FIGURE 17: Distribution maps of virus-laden particles inside the elevator at 120 s after the infected person coughs, considering differences in body type between source and exposed individual.

since the particle cloud cannot reach the breathing zone of the exposed person, the exposure probability is close to 0. If the child is the source of infection, it is absolutely safe to keep a distance of more than 1.5 m from him in an elevator.

3.8. Discussion. This study's simulation is based on several key assumptions that influence the results and interpretations. These assumptions are essential for simplifying the complex dynamics of virus transmission in an elevator environment and making the computational model feasible. Below, we outline and analyze these assumptions:

- Uniform virus load distribution: The assumption is made that the virus load in droplets is uniformly distributed, with a baseline virus load set to 10^9 copies/mL. This assumption simplifies the modeling of viral concentration in droplets but may not fully capture the variability in virus load observed in the real world, where viral loads can differ greatly between individuals and over time.
- Fixed airflow field: Before activating the DPM, it is assumed that the airflow field inside the elevator is in a stable fixed state. This assumption allows for the establishment of a stable baseline for simulating droplet diffusion but may overlook instantaneous airflow changes caused by elevator movement or door operation. Moreover, the elevator's ascent and descent can induce positive and negative pressures, influencing the ventilation rate. Future studies could explore this aspect further.
- Simplified breathing patterns: The study uses predefined particle size distributions and velocities to simulate specific breathing patterns (coughing, sneezing, loud talking, and continuous coughing). While these patterns are based on empirical data, they do not account for individual variations in breathing behavior or the possibility of mixed respiratory activities.
- Neglecting short-term virus viability: The simulation assumes constant virus survival rates in aerosols during the short exposure period. This assumption is reasonable for brief exposure scenarios but may not hold for longer exposure times, where the virus viability might decrease.
- Uniform environmental conditions: The study assumes constant temperature and relative humidity inside the elevator, based on typical design standards. This assumption may not capture dynamic environmental changes in different elevator settings or due to external factors.
- Fixed body position and height: The position and height of individuals in the elevator are assumed to be fixed, with no consideration of movement or posture changes. This assumption simplifies the geometric model but may not reflect behavioral variations in confined spaces. Additionally, the position and number of individuals in the elevator are randomly assigned, and the likelihood of inhaling virus-laden aerosols differs when individuals face the source compared to when they are turned away. Future analyses should explore the infection probability under varying numbers of people, standing postures, and positions.
- Fixed heat flux body model: In reality, the skin temperature and heat radiation from different body parts vary, and clothing materials have different insulation properties. These factors influence buoyant effects around the body caused by thermal plumes. Future research should delve deeper into the impact of varying heat flux.

By acknowledging these assumptions, the study provides a framework for understanding the limitations of future research and potential areas for improvement. Addressing these assumptions in subsequent studies can enhance the accuracy and applicability of the results to real-world scenarios.

In addition to the limitations based on assumptions, we focus on issues such as computational constraints, data accuracy, model validation, and scalability.

- Computational constraints: The study investigates the impact of environmental variables such as temperature, relative humidity, and ventilation rate gradients

on SARS-CoV-2 transmission risk. Due to computational resource limitations, the range of variable variations used in this study is still broad and may not fully capture all potential nuances and complexities. To overcome these limitations, future research could incorporate machine learning techniques. As a powerful data-driven predictive tool, machine learning can handle large, complex datasets and extract valuable patterns and insights. By applying machine learning algorithms, the impact of environmental variables on virus transmission can be analyzed more accurately, optimizing ventilation strategies and reducing the risk of viral spread.

- Data accuracy: Given the number of factors considered in this study, future research should incorporate sensitivity analysis to comprehensively assess the impact of different parameters on the results' accuracy and identify the factors that most influence infection risk.
- Scalability issues: The model is specifically designed for elevator environments and may not be directly applicable to other settings without significant modifications. The assumptions and parameters used may not be suitable for larger or differently configured spaces. Future studies should focus on developing models that are adaptable to a broader range of environments.

Addressing these limitations in future research can improve the accuracy and applicability of the results, providing more reliable insights into virus transmission dynamics in confined spaces.

The findings of this study offer valuable insights into the transmission dynamics of SARS-CoV-2 in elevator environments. Below are specific examples of potential applications in industries, policymaking, and engineering, as well as potential limitations and considerations:

- In elevator design and engineering, the results of this study suggest that optimizing ventilation systems could reduce transmission risk. However, practical implementation must consider existing building codes, structural constraints, and cost implications. Retrofitting old elevators with new ventilation systems may present practical challenges.
- In public health policy and guidelines, policymakers could develop guidelines for the safe use of elevators during pandemics. However, these guidelines must be adaptable to different building types and occupancy patterns. Compliance and enforcement may vary, impacting the effectiveness of the measures.

4. Concluding Remarks

This study simulates aerosol transmission during a 2-min elevator ride with two individuals facing each other, without considering the use of masks. Through analysis of the infection probabilities faced by exposed individuals with three different virus strains, as well as the purification capabilities of the elevator space ventilation system, the following conclusions have been drawn:

- The top-to-bottom airflow design in elevator ventilation systems poses the lowest risk. Except for the Omicron variant, the chance of infection with other virus strains remains below 40% for those exposed. On the other hand, having the exit at the top leads to the highest accumulation of virus particles inhaled, increasing the risk of transmission.
- Breathing through the nose rather than the mouth can reduce virus intake. Increasing the ventilation rate helps accelerate the removal of particles in an elevator. Raising the ventilation rate to 30 ACH effectively purifies the air and significantly reduces the cumulative dose of inhaled viruses.
- Temperature and relative humidity fluctuations also affect the spread of virus particles. At an ambient temperature of 27°C, a large amount of particles will accumulate in the breathing zone of the exposed person, increasing the risk of inhaling the virus. However, when the ambient temperature exceeds body temperature, the probability of infection of the exposed person is almost zero. Increasing the relative humidity to 95% slightly reduces the probability of infection, achieving the best effect among the conditions studied.
- Distributed ACV systems demonstrate optimal cleaning efficiency, with a threefold improvement compared to side ventilation systems. Among all ACV methods at an air change rate (ACH) of 20, the probability of infection for exposed individuals does not exceed 50%, except when facing the Omicron variant. This highlights the critical role of efficient ventilation methods in reducing transmission risks.
- When an infected person sneezes, the level of virus inhalation for those exposed is higher by 1–2 orders of magnitude compared to other respiratory modes, resulting in a 99% infection probability for all viral strains. In contrast, speaking loudly leads to minimal virus intake for exposed individuals, maintaining infection probabilities for all viral strains below 20%.
- People who are shorter in height face higher risks, with infection probabilities nearing 99% for those 1.3 and 1.55 m tall. Particles generated by children have the least impact on the exposed individual. This underscores the importance of considering height differentials between infected and exposed individuals when assessing transmission risks.

In summary, analyzing the influence of various factors on virus transmission inside elevators can provide insights into improving elevator ventilation systems and usage behaviors to reduce the risk of infection for occupants. These research findings are crucial for establishing elevator usage guidelines and enhancing ventilation system designs.

Appendix I: Distribution Maps of Virus-Laden Particles Inside the Elevator Over Time at Different Ventilation Methods

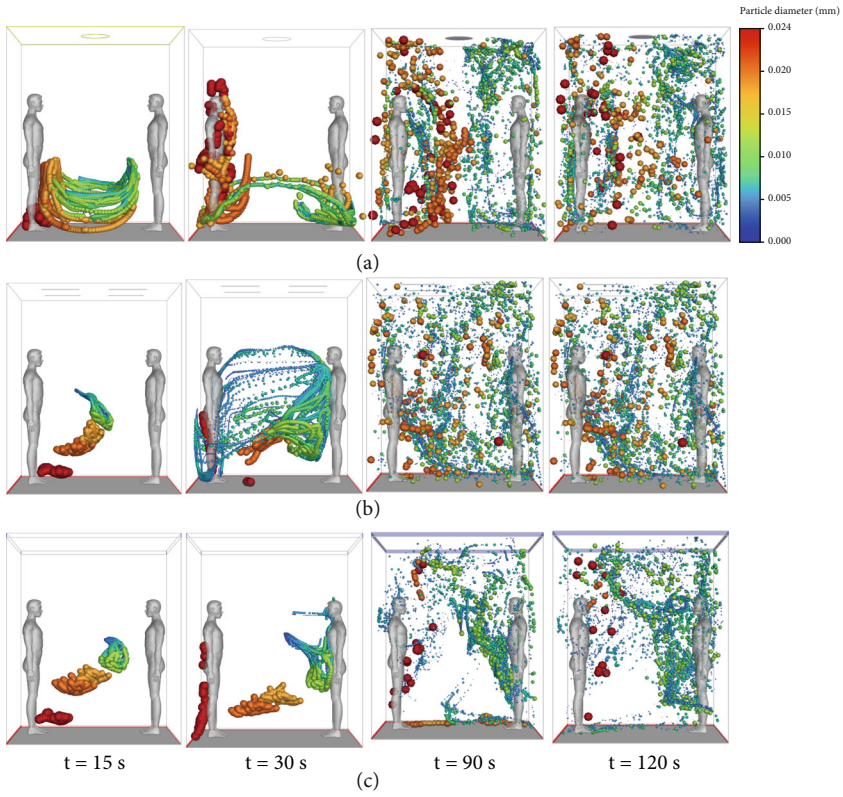

Figure A1: Distribution maps of virus-laden particles inside the elevator over time at different ventilation methods. (a) Central air curtain type. (b) Distributed air curtain type. (c) Side ventilation method.

Appendix II: Histograms of Position Distribution of Particles Inside Elevator at 120 s Under Different Cases

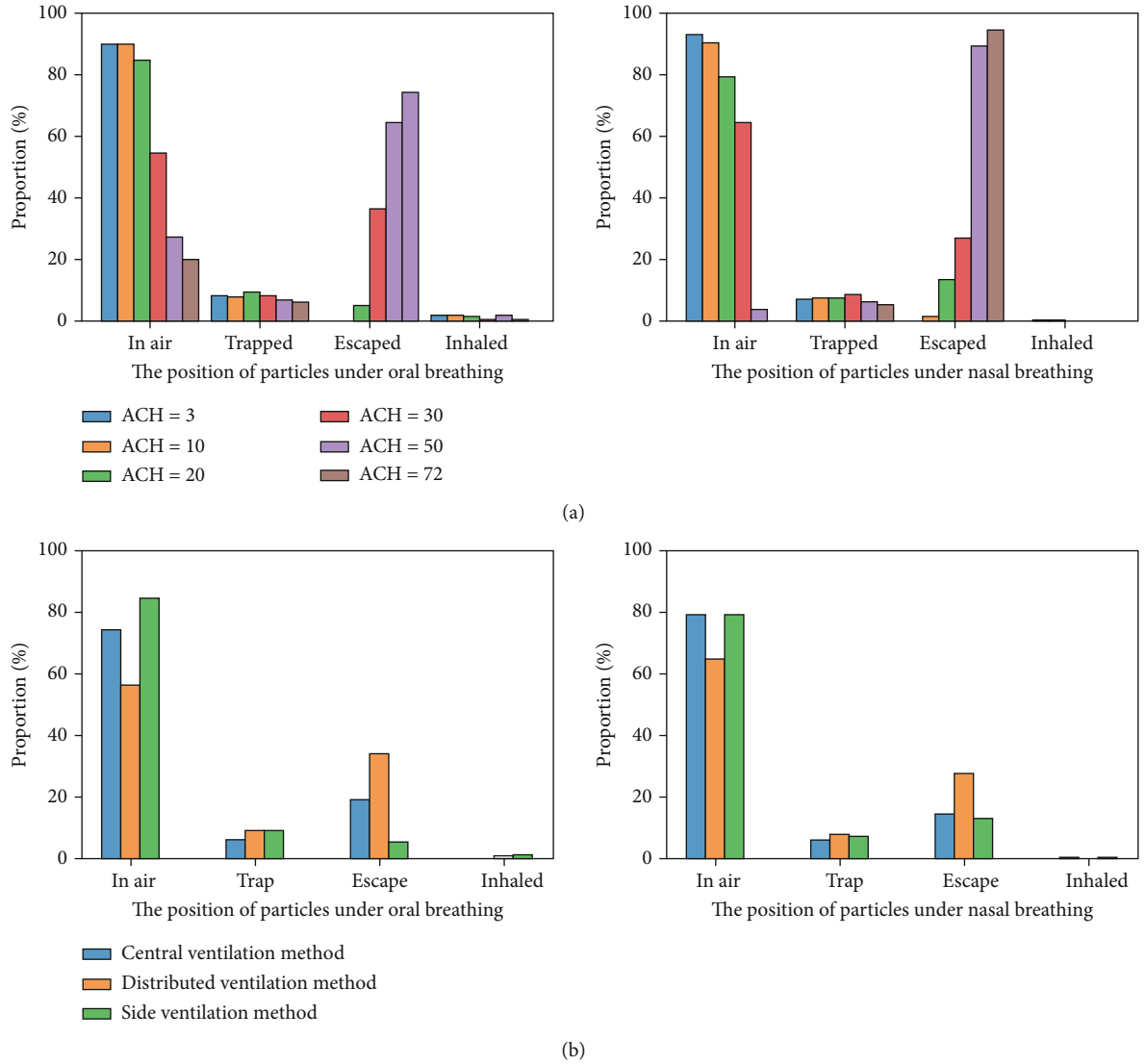

Figure A2: Histograms of position distribution of particles inside the elevator at 120 s under different cases. (a) Under different ventilation volumes. (b) Under different ventilation methods (VMs).

Appendix III: Cumulative Virus Inhalation of Individual Exposed to Oral and Nasal Breathing Over Time Under Different Cases

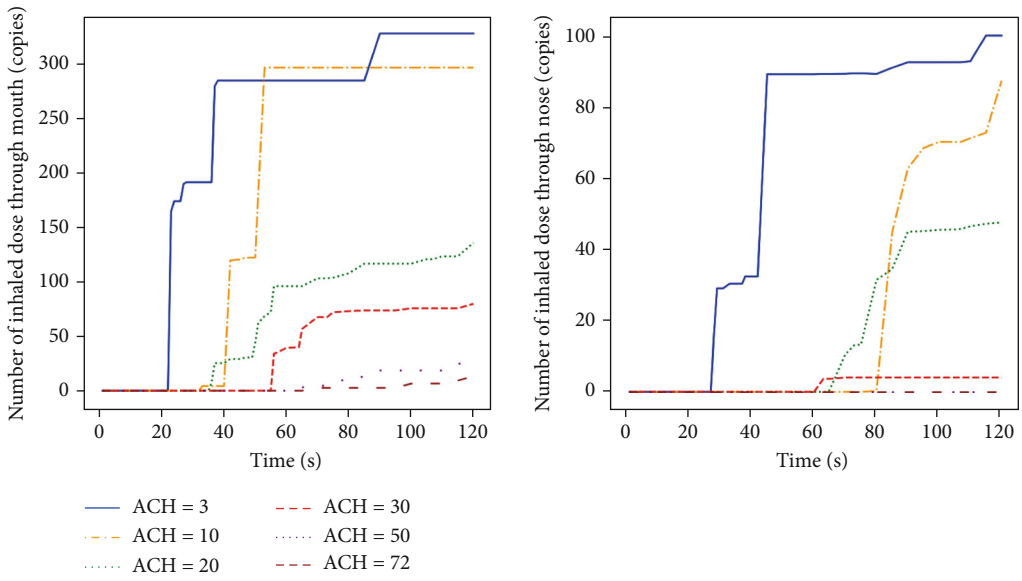

(a)

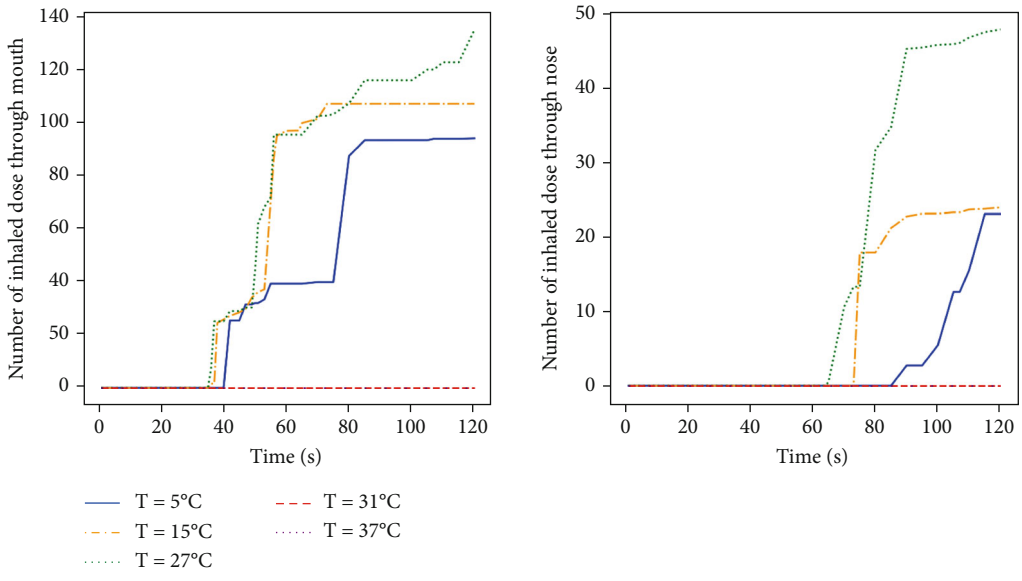

(b)

Figure A3: Continued.

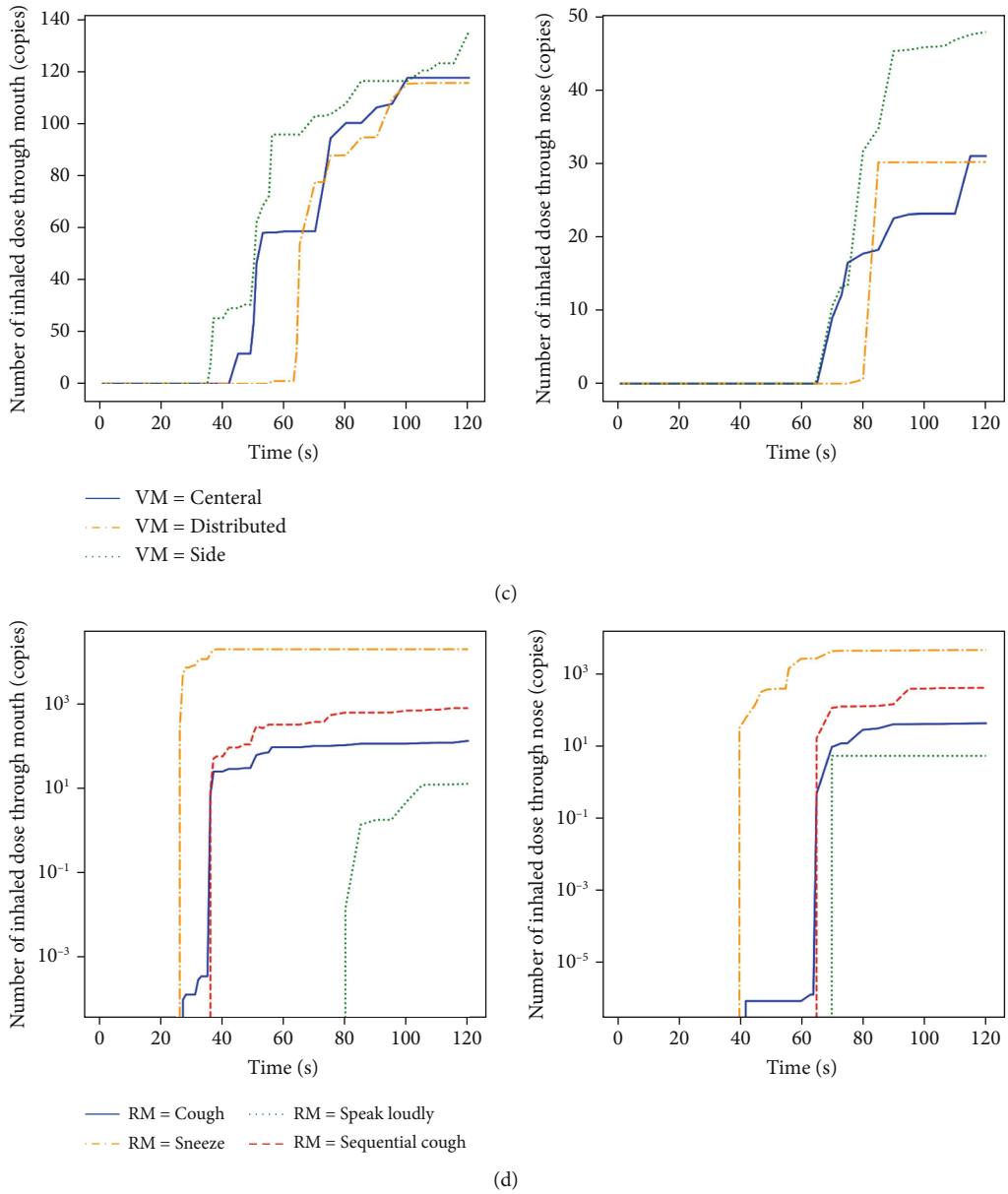

FIGURE A3: Cumulative virus inhalation of individual exposed to oral and nasal breathing over time under different cases. (a) Under different ventilation volumes. (b) Under different temperatures (T). (c) Under different ventilation methods (VMs). (d) Under different respiratory patterns.

Appendix IV: Analysis of Infection Probability of Exposed Individual Under Different Cases

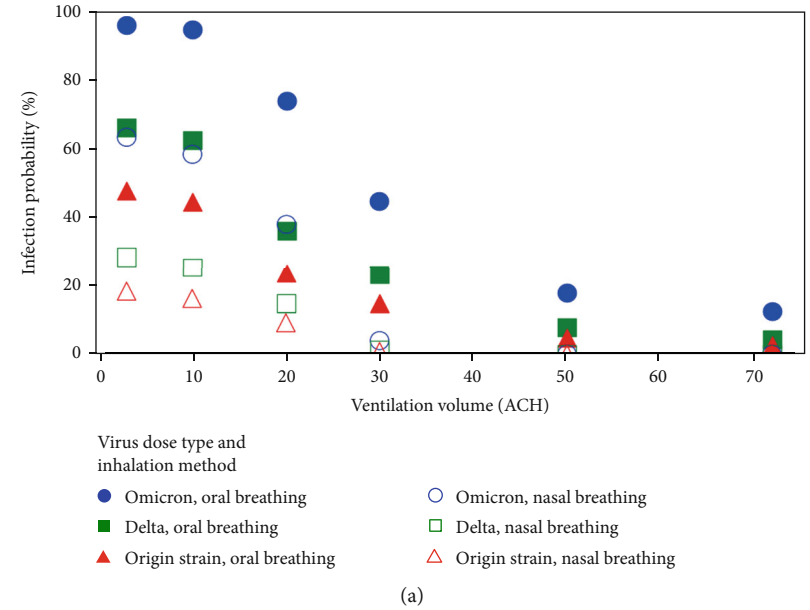

(a)

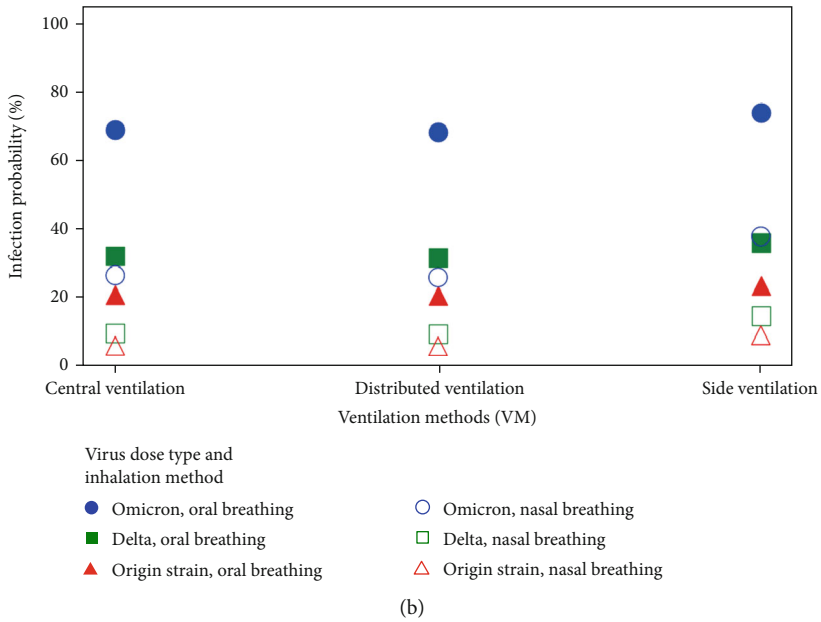

(b)

Figure A4: Continued.

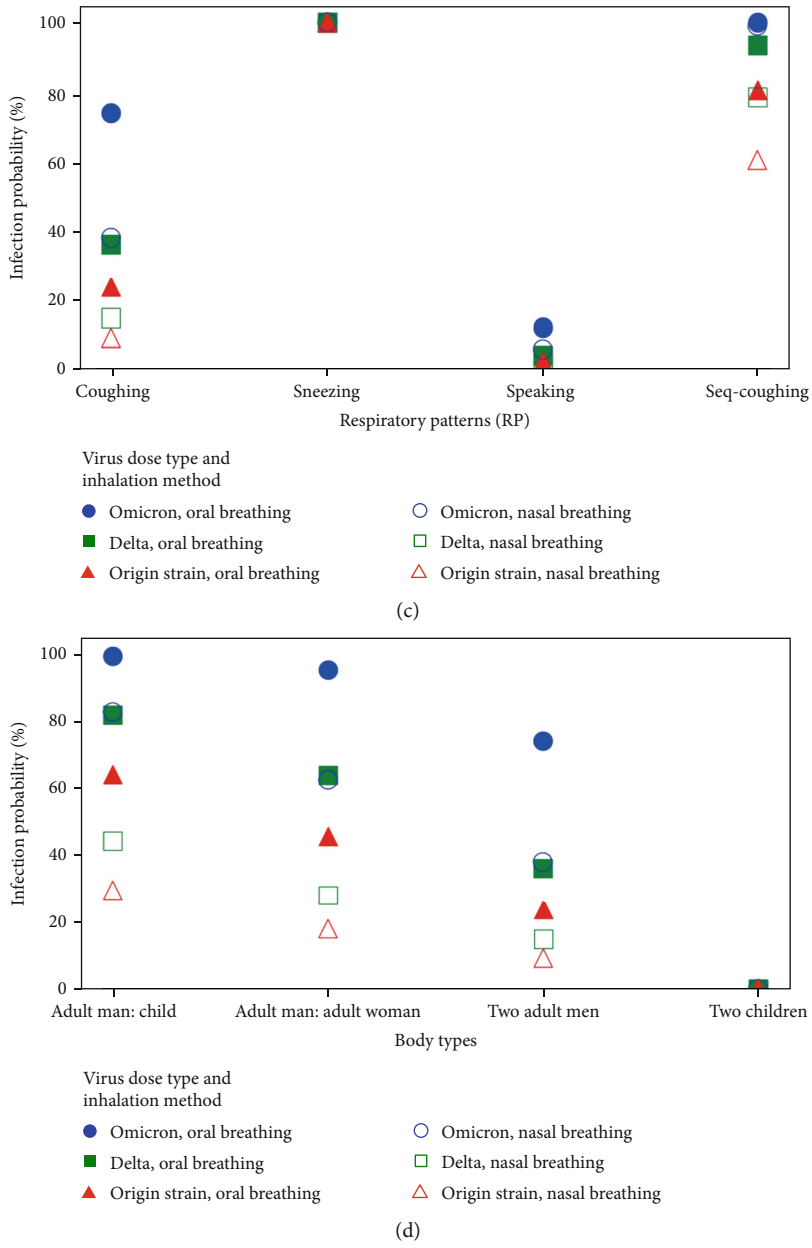

Figure A4: Analysis of infection probability of exposed individual under different cases. (a) Under different ACH. (b) Under different ventilation methods (VMs). (c) Under different respiratory patterns (RPs) of infected individual. (d) Under different body types.

Data Availability Statement

The data that support the findings of this study are available from the corresponding author upon reasonable request.

Conflicts of Interest

The authors declare no conflicts of interest.

Funding

This investigation is supported by research funding from the Ministry of Education (MOE) of Singapore under grant number T2EP50221-0042. The financial support provided by the Hong Kong Polytechnic University in the form of a postgraduate scholarship for the first author is also gratefully acknowledged.

References

[1] S. Taylor, "The Psychology of Pandemics," *Annual Review of Clinical Psychology* 18, no. 1 (2022): 581–609, https://doi.org/10.1146/annurev-clinpsy-072720-020131.

[2] C. W. Rudolph, B. Allan, M. Clark, et al., "Pandemics: Implications for Research and Practice in Industrial and Organizational Psychology," *Industrial and Organizational Psychology* 14, no. 1-2 (2021): 1–35, https://doi.org/10.1017/iop.2020.48.

[3] "WHO Coronavirus (COVID-19) Dashboard," WHO.int, 2025), Available: https://covid19.who.int/ [Accessed: 26-March -2025].

[4] W. Chen, N. Zhang, J. Wei, H. L. Yen, and Y. Li, "Short-Range Airborne Route Dominates Exposure of Respiratory Infection During Close Contact," *Building and Environment* 176 (2020): 106859, https://doi.org/10.1016/j.buildenv.2020.106859.

[5] C. C. Wang, K. A. Prather, J. Sznitman, et al., "Airborne Transmission of Respiratory Viruses," *Science* 373, no. 6558 (2021): eabd9149, https://doi.org/10.1126/science.abd9149.

[6] M. Cevik, K. Kuppalli, J. Kindrachuk, and M. Peiris, "Virology, Transmission, and Pathogenesis of SARS-CoV-2," *BMJ* 371 (2020): m3862, https://doi.org/10.1136/bmj.m3862.

[7] J. P. Duguid, "The Size and the Duration of Air-Carriage of Respiratory Droplets and Droplet-Nuclei," *Epidemiology & Infection* 44, no. 6 (1946): 471–479, https://doi.org/10.1017/S0022172400019288.

[8] C. Y. Chao and M. P. Wan, "A Study of the Dispersion of Expiratory Aerosols in Unidirectional Downward and Ceiling-Return Type Airflows Using a Multiphase Approach," *Indoor Air* 16, no. 4 (2006): 296–312, https://doi.org/10.1111/j.1600-0668.2006.00426.x.

[9] G. Busco, S. R. Yang, J. Seo, and Y. A. Hassan, "Sneezing and Asymptomatic Virus Transmission," *Physics of Fluids* 32, no. 7 (2020): 073309, https://doi.org/10.1063/5.0019090.

[10] M. Han, R. Ooka, H. Kikumoto, W. Oh, Y. Bu, and S. Hu, "Experimental Measurements of Airflow Features and Velocity Distribution Exhaled From Sneeze and Speech Using Particle Image Velocimetry," *Building and Environment* 205 (2021): 108293, https://doi.org/10.1016/j.buildenv.2021.108293.

[11] R. Wölfel, V. M. Corman, W. Guggemos, et al., "Virological Assessment of Hospitalized Patients With COVID-2019," *Nature* 581, no. 7809 (2020): 465–469, https://doi.org/10.1038/s41586-020-2196-x.

[12] Z. Li, H. Wang, X. Zhang, T. Wu, and X. Yang, "Effects of Space Sizes on the Dispersion of Cough-Generated Droplets From a Walking Person," *Physics of Fluids* 32, no. 12 (2020): 121705, https://doi.org/10.1063/5.0034874.

[13] Y. Li, H. Qian, J. Hang, et al., "Probable Airborne Transmission of SARS-CoV-2 in a Poorly Ventilated Restaurant," *Building and Environment* 196 (2021): 107788, https://doi.org/10.1016/j.buildenv.2021.107788.

[14] C. Xie, H. Zhao, K. Li, et al., "The Evidence of Indirect Transmission of SARS-CoV-2 Reported in Guangzhou, China," *BMC Public Health* 20, no. 1 (2020): 1202, https://doi.org/10.1186/s12889-020-09296-y.

[15] N. Izadyar and W. Miller, "Ventilation Strategies and Design Impacts on Indoor Airborne Transmission: A Review," *Building and Environment* 218 (2022): 109158, https://doi.org/10.1016/j.buildenv.2022.109158.

[16] The American Society of Mechanical Engineers, "ASME A17.1/CSA B44-16. Safety Code for Elevators and Escalators" 2019, Available: https://www.asme.org/getmedia/05d3cb98-f573-42f4-b8ad-86a26682091a/a17-1_csa-b44_2019-table-of-contents.pdf. [Accessed: 03 - May -2025].

[17] ISO 8100-1, *Lifts for the Transport of Persons and Goods — Part 1: Passenger and Goods Passenger Lifts* (International Standards Organisation, 2009), Available: https://www.iso.org/standard/70824.html.[Accessed: 23- Jul -2024].

[18] GN1240, *Code of Practice on the Design and Construction of Lifts and Escalators (2021 Edition)* (Electrical and Mechanical Services Development, The Government of Hong Kong, 2021), Available: https://www.emsd.gov.hk/tc/lifts_and_escalators_safety/publications/code_of_practice. [Accessed: 11 - Jul - 2024].

[19] C. van Rijn, G. A. Somsen, L. Hofstra, et al., "Reducing Aerosol Transmission of SARS-CoV-2 in Hospital Elevators," *Indoor Air* 30, no. 6 (2020): 1065–1066, https://doi.org/10.1111/ina.12744.

[20] S. Shao, D. Zhou, R. He, et al., "Risk Assessment of Airborne Transmission of COVID-19 by Asymptomatic Individuals Under Different Practical Settings," *Journal of Aerosol Science* 151 (2021): 105661, https://doi.org/10.1016/j.jaerosci.2020.105661.

[21] N. Sen, "Transmission and Evaporation of Cough Droplets in an Elevator: Numerical Simulations of Some Possible Scenarios," *Physics of Fluids* 33, no. 3 (2021): 033311, https://doi.org/10.1063/5.0039559.

[22] R. Biswas, A. Pal, R. Pal, S. Sarkar, and A. Mukhopadhyay, "Risk Assessment of COVID Infection by Respiratory Droplets From Cough for Various Ventilation Scenarios Inside an Elevator: An OpenFOAM-Based Computational Fluid Dynamics Analysis," *Physics of Fluids* 34, no. 1 (2022): 013318, https://doi.org/10.1063/5.0073694.

[23] T. Dbouk and D. Drikakis, "On Airborne Virus Transmission in Elevators and Confined Spaces," *Physics of Fluids* 33, no. 1 (2021): 011905, https://doi.org/10.1063/5.0038180.

[24] X. Li and B. Feng, "Transmission of Droplet Aerosols in an Elevator Cabin: Effect of the Ventilation Mode," *Building and Environment* 236 (2023): 110261, https://doi.org/10.1016/j.buildenv.2023.110261.

[25] S. Liu and Z. Deng, "Transmission and Infection Risk of COVID-19 When People Coughing in an Elevator," *Building and Environment* 238 (2023): 110343, https://doi.org/10.1016/j.buildenv.2023.110343.

[26] ISO 5151-2017, *Non-Ducted Air Conditioners and Heat Pumps — Testing and Rating for Performance* (International Standards Organisation, 2017), Available: https://www.iso.org/standard/63409.html. [Accessed: 11 - Aug - 2024].

[27] ANSI/ASHRAE Standard 62.1-2022, *Ventilation and Acceptable Indoor Air Quality* (American Society of Heating, Refrigerating and Air-Conditioning Engineers, 2022), Available: https://ashrae.iwrapper.com/ASHRAE_PREVIEW_ONLY_STANDARDS/STD_62.1_2022. [Accessed: 11- Dec -2024].

[28] T. A. Popov, T. Z. Kralimarkova, M. Labor, and D. Plavec, "The Added Value of Exhaled Breath Temperature in Respiratory Medicine," *Journal of Breath Research* 11, no. 3 (2017): 034001, https://doi.org/10.1088/1752-7163/aa7801.

[29] E. Mansour, R. Vishinkin, S. Rihet, et al., "Measurement of Temperature and Relative Humidity in Exhaled Breath," *Sensors and Actuators B: Chemical* 304 (2020): 127371, https://doi.org/10.1016/j.snb.2019.127371.

[30] J. K. Gupta, C. H. Lin, and Q. Chen, "Characterizing Exhaled Airflow From Breathing and Talking," *Indoor Air* 20, no. 1 (2010): 31–39, https://doi.org/10.1111/j.1600-0668.2009.00623.x.

[31] J. K. Gupta, C. H. Lin, and Q. Chen, "Flow Dynamics and Characterization of a Cough," *Indoor Air* 19, no. 6 (2009): 517–525, https://doi.org/10.1111/j.1600-0668.2009.00619.x.

[32] V. Stadnytskyi, P. Anfinrud, and A. Bax, "Breathing, Speaking, Coughing or Sneezing: What Drives Transmission of SARS-CoV-2?," *Journal of Internal Medicine* 290, no. 5 (2021): 1010–1027, https://doi.org/10.1111/joim.13326.

[33] A. Fluent, *Ansys Fluent Theory Guide* 15317, Ansys Inc., 2011).

[34] V. S. A. S. T. B. C. G. Yakhot, S. A. Orszag, S. Thangam, T. B. Gatski, and C. Speziale, "Development of Turbulence Models for Shear Flows by a Double Expansion Technique," *Physics of Fluids a: Fluid Dynamics* 4, no. 7 (1992): 1510–1520, https://doi.org/10.1063/1.858424.

[35] E. C. Riley, G. Murphy, and R. L. Riley, "Airborne Spread of Measles in a Suburban Elementary School," *American Journal of Epidemiology* 107, no. 5 (1978): 421–432, https://doi.org/10.1093/oxfordjournals.aje.a112560.

[36] R. Clift, J. R. Grace, and M. E. Weber, *Bubbles, Drops, and Particles* (Dover Publications, Inc., 2005).

[37] F. Carrouel, E. Gadea, A. Esparcieux, et al., "Saliva Quantification of SARS-CoV-2 in Real-Time PCR From Asymptomatic or Mild COVID-19 Adults," *Frontiers in Microbiology* 12 (2022): 786042, https://doi.org/10.3389/fmicb.2021.786042.

[38] T. C. Jones, G. Biele, B. Mühlemann, et al., "Estimating Infectiousness Throughout SARS-CoV-2 Infection Course," *Science* 373, no. 6551 (2021): eabi5273, https://doi.org/10.1126/science.abi5273.

[39] S. Anand and Y. S. Mayya, "Size Distribution of Virus Laden Droplets From Expiratory Ejecta of Infected Subjects," *Scientific Reports* 10, no. 1 (2020): 21174, https://doi.org/10.1038/s41598-020-78110-x.

[40] S. Basu, "Computational Characterization of Inhaled Droplet Transport to the Nasopharynx," *Scientific Reports* 11, no. 1 (2021): 6652, https://doi.org/10.1038/s41598-021-85765-7.

[41] "Understanding Transmission of SARS-CoV-2 in the Ongoing COVID-19 Pandemic," NCCEH.ca, 2023), Available: https://ncceh.ca/resources/evidence-reviews/understanding-transmission-sars-cov-2-ongoing-covid-19-pandemic#h3-4. [Accessed: 1 - Aug -2024].

[42] "Master Question List for COVID-19 (Caused by SARS-CoV-2)," DHS.gov, 2023), Available: https://www.dhs.gov/publication/st-master-question-list-covid-19. [Accessed: 1-Aug -2024].

[43] G. N. Sze To and C. Y. H. Chao, "Review and Comparison Between the Wells–Riley and Dose-Response Approaches to Risk Assessment of Infectious Respiratory Diseases," *Indoor air* 20, no. 1 (2010): 2–16, https://doi.org/10.1111/j.1600-0668.2009.00621.x.

[44] S. Liu, X. Zhao, S. R. Nichols, et al., "Evaluation of Airborne Particle Exposure for Riding Elevators," *Building and Environment* 207 (2022): 108543, https://doi.org/10.1016/j.buildenv.2021.108543.

[45] N. M. Zahari, M. H. Zawawi, L. M. Sidek, et al., "Introduction of Discrete phase Model (DPM) in Fluid Flow: A Review," *AIP Conference Proceedings* 2030, no. 1 (2018): 020234, https://doi.org/10.1063/1.5066875.

[46] A. C. Lowen, S. Mubareka, J. Steel, and P. Palese, "Influenza Virus Transmission Is Dependent on Relative Humidity and Temperature," *PLoS Pathogens* 3, no. 10 (20071470–1476, e151, https://doi.org/10.1371/journal.ppat.0030151.

[47] M. Wang, A. Jiang, L. Gong, et al., "Temperature Significantly Change COVID-19 Transmission in 429 Cities," *Medrxiv* (2020): https://doi.org/10.1101/2020.02.22.20025791.

[48] M. Y. Chong, H. An, S. Kanagalingam, et al., "Influence of the Occupant's Height on Cough Dispersion and Infection Risk Within an Indoor Environment: A Numerical Study," in *ASTFE Digital Library* (Begel House Inc., 2024), https://doi.org/10.1615/TFEC2024.bio.050579.